Stability analysis of the inverse Lax-Wendroff boundary treatment for high order central difference schemes for diffusion equations

Tingting Li[1], Chi-Wang Shu[2] and Mengping Zhang[3]

Abstract

In this paper, high order central finite difference schemes in a finite interval are analyzed for the diffusion equation. Boundary conditions of the initial-boundary value problem (IBVP) are treated by the simplified inverse Lax-Wendroff (SILW) procedure. For the fully discrete case, a third order explicit Runge-Kutta method is used as an example for the analysis. Stability is analyzed by both the GKS (Gustafsson, Kreiss and Sundström) theory and the eigenvalue visualization method on both semi-discrete and fully discrete schemes. The two different analysis techniques yield consistent results. Numerical tests are performed to demonstrate and validate the analysis results.

Key Words: high order central difference schemes; diffusion equation; simplified inverse Lax-Wendroff procedure; stability; GKS theory; eigenvalue analysis.

[1]School of Mathematical Sciences, University of Science and Technology of China, Hefei, Anhui 230026, P.R. China. E-mail: ltt1120@mail.ustc.edu.cn

[2]Division of Applied Mathematics, Brown University, Providence, RI 02912, USA. E-mail: shu@dam.brown.edu. Research supported by AFOSR grant F49550-12-1-0399 and NSF grant DMS-1418750.

[3]School of Mathematical Sciences, University of Science and Technology of China, Hefei, Anhui 230026, P.R. China. E-mail: mpzhang@ustc.edu.cn. Research supported by NSFC grant 11471305.

1 Introduction

High order finite difference schemes with wide stencils to solve diffusion equations cannot be used directly near the boundaries. Two problems in obtaining numerical boundary conditions near the boundaries should be addressed properly in order to maintain accuracy and stability. Firstly, the points used in these schemes which lie outside the computational domain, namely the "ghost points", should be evaluated properly. Secondly, the grid points may not coincide with the physical boundary exactly. This would be the case when a cartesian mesh is used to solve problems on complex geometry. There are many methods in the literature for handling boundary conditions on irregular domains, see for example [1, 9, 10, 11, 17]. Stability is always a major concern. This is especially the case when the first grid point does not coincide with but is very close to the physical boundary (relative to the mesh size inside the domain), which is referred to in the literature as the "cut-cell" problem [1]. Such "cut-cell" situation is difficult to avoid during mesh refinement, and special attention is needed in order to overcome possible instability. The simplified inverse Lax-Wendroff (SILW) procedure, first introduced in [23] for hyperbolic equations, can be used to overcome these difficulties. For earlier related work, see [3, 4, 7, 6, 8, 21, 22]. Recently, this technique has been extended to convection-diffusion equations in [14]. In this paper, we would like to analyze stability for the extension of this technique to diffusion equations.

General stability analysis for initial boundary value problems (IBVP) on a finite domain can be performed by the famous Gustafsson, Kreiss and Sundström (GKS) theory [5]. For parabolic problems considered in this paper, such stability analysis was formulated in, e.g. [24, 15, 18]. In [5], stability analysis is performed for fully discrete finite difference schemes. Later in [19], stability analysis is performed for the semi-discrete cases. A drawback of the GKS analysis is the high algebraic complexity in the case of very high order accuracy. An alternative technique, by visualizing the eigenvalue spectrum of the discretization operators, which was adopted in [25], could also be used to

analyze stability. It has been observed in [25] that, when both techniques are used, they produce consistent stability conclusions. In our earlier work [12], we systematically studied stability for high order upwind-biased finite difference schemes for hyperbolic equations, using these two techniques. The minimum number of inverse Lax-Wendroff terms needed for stability is documented for schemes of various order of accuracy with the SILW procedure. In this paper, we would like to extend our work in [12] to study the stability of semi-discrete and fully discrete high order central finite difference schemes for diffusion equations. The SILW procedure will be used near the boundaries. Both the GKS analysis and the eigenvalue analysis will be performed. Even though we only consider pure diffusion equations in this paper, our eventual objective is to use the methodology for convection dominated convection-diffusion equations, thus justifying the choice of explicit time-stepping methods for the analysis.

This paper is organized as follows. In Section 2, we review high order central finite difference methods as the inner schemes, and the third order total variation diminishing (TVD) Runge-Kutta time discretization method used in the fully discrete problems. The SILW procedure is introduced in detail in this section as well. Stability analysis is performed in Section 3 by using the GKS theory and the eigenvalue spectrum method, first for the semi-discrete case and then for the fully discrete case. Numerical tests are provided in Section 4 to demonstrate and validate the results of the analysis. Concluding remarks are given in Section 5.

2 Scheme formulation

In this section, we review high order central finite difference methods as the inner schemes. The third order explicit total variation diminishing (TVD) Runge-Kutta time discretization method [16] is used in the full discretization. The SILW procedure used in the boundary treatments will be stated in detail in this section.

2.1 High order central difference schemes

Consider the one-dimensional scalar diffusion equation

$$\begin{cases} u_t = c\ u_{xx},\ x \in [a,b],\ t \geq 0 \\ u(x,0) = u_0(x),\ x \in [a,b] \end{cases} \tag{2.1}$$

with Dirichlet boundary conditions

$$\begin{cases} u(a,t) = g_1(t),\ t \geq 0 \\ u(b,t) = g_2(t),\ t \geq 0 \end{cases} \tag{2.2}$$

or Neumann boundary conditions

$$\begin{cases} u_x(a,t) = g_3(t),\ t \geq 0 \\ u_x(b,t) = g_4(t),\ t \geq 0 \end{cases} \tag{2.3}$$

Here, $c > 0$, which is restricted by the well-posedness of the IBVP (2.1).

The interval (a,b) is discretized by a uniform mesh as

$$a + C_a\ \Delta x = x_0 < x_1 < x_2 < \cdots < x_N = b - C_b\ \Delta x \tag{2.4}$$

where $C_a \in [0,1)$ and $C_b \in [0,1)$. $\{x_j = a + (C_a + j)\ \Delta x,\ j = 0,1,2,\cdots N\}$ are the grid points. The first and the last grid points are not necessarily aligned with the boundary, and we choose this kind of discretization on purpose. Such non-alignment would be difficult to avoid in multi-dimensions when cartesian meshes are used to solve problems in complex geometry. It is also difficult to avoid even in one-dimension if the computational domain moves with time.

The general semi-discrete conservative finite difference scheme approximating (2.1), based on point values and numerical fluxes, is of the form:

$$\frac{du_j}{dt} = \frac{c}{\Delta x^2}\ (\hat{v}_{j+\frac{1}{2}}(t) - \hat{v}_{j-\frac{1}{2}}(t)) \tag{2.5}$$

where the numerical flux $\hat{v}_{j+\frac{1}{2}}$ is defined as a linear combination of $u(x,t)$ in the neighborhood of x_j such that the right hand of (2.5) approximates cu_{xx} at $x = x_j$ to the desired order of accuracy. The numerical flux $\hat{v}_{j+\frac{1}{2}}$ can be obtained either with constant

coefficient linear approximations or with weighted essentially non-oscillatory (WENO) approximations [13], which is useful for nonlinear degenerate parabolic equations with possibly discontinuous solutions. In this paper we only consider constant coefficient linear approximations, hence the semi-discrete approximation (2.5) can be written as

$$\frac{du_j}{dt} = \frac{c}{\Delta x^2}\mathcal{D}_{j,\hat{k},\hat{m}} \cdot u_j \equiv \frac{c}{\Delta x^2}\sum_{l=0}^{\hat{m}} d_{\hat{k},l}\; u_{j-\hat{k}+l} \tag{2.6}$$

where $j-\hat{k}$ denotes the left most point of the stencil having $\hat{m}+1$ points, and $d_{\hat{k},l}$ are constants. Both $\hat{k}$ and $\hat{m}$ depend on the order of the scheme.

Schemes considered in this paper are listed below.

- The second order scheme

$$\frac{du_j}{dt} = \frac{c}{\Delta x^2}\;(u_{j+1} - 2u_j + u_{j-1})$$

- The fourth order scheme

$$\frac{du_j}{dt} = \frac{c}{\Delta x^2}\;(-\frac{1}{12}u_{j-2} + \frac{4}{3}u_{j-1} - \frac{5}{2}u_j + \frac{4}{3}u_{j+1} - \frac{1}{12}u_{j+2})$$

- The sixth order scheme

$$\frac{du_j}{dt} = \frac{c}{\Delta x^2}\;(\frac{1}{90}u_{j-3} - \frac{3}{20}u_{j-2} + \frac{3}{2}u_{j-1} - \frac{49}{18}u_j + \frac{3}{2}u_{j+1} - \frac{3}{20}u_{j+2} + \frac{1}{90}u_{j+3})$$

- The eighth order scheme

$$\begin{aligned}\frac{du_j}{dt} = \frac{c}{\Delta x^2}\;(&-\frac{1}{560}u_{j-4} + \frac{8}{315}u_{j-3} - \frac{1}{5}u_{j-2} + \frac{8}{5}u_{j-1} - \frac{205}{72}u_j \\ &+ \frac{8}{5}u_{j+1} - \frac{1}{5}u_{j+2} + \frac{8}{315}u_{j+3} - \frac{1}{560}u_{j+4})\end{aligned}$$

- The tenth order scheme

$$\begin{aligned}\frac{du_j}{dt} = \frac{c}{\Delta x^2}\;(&\frac{1}{3150}u_{j-5} - \frac{5}{1008}u_{j-4} + \frac{5}{126}u_{j-3} - \frac{5}{21}u_{j-2} + \frac{5}{3}u_{j-1} - \frac{5269}{1800}u_j \\ &+ \frac{5}{3}u_{j+1} - \frac{5}{21}u_{j+2} + \frac{5}{126}u_{j+3} - \frac{5}{1008}u_{j+4} + \frac{1}{3150}u_{j+5})\end{aligned}$$

All schemes are centered at the grid point x_j and they are thus central difference schemes.

In the fully discrete schemes, a third order explicit TVD Runge-Kutta time discretization method [16] is used as an example. For simplicity, the semi-discrete schemes are written as

$$u_t = \mathcal{L}u$$

From the time level t_n to t_{n+1}, the third order TVD Runge-Kutta method is given by

$$\begin{aligned} u^{(1)} &= u^n + \Delta t \mathcal{L}(u^n) \\ u^{(2)} &= \frac{3}{4}u^n + \frac{1}{4}u^{(1)} + \frac{1}{4}\Delta t \mathcal{L}(u^{(1)}) \\ u^{n+1} &= \frac{1}{3}u^n + \frac{2}{3}u^{(2)} + \frac{2}{3}\Delta t \mathcal{L}(u^{(2)}) \end{aligned}$$

where Δt is the time step.

Special attention must be taken when we impose time dependent boundary conditions in the two interior stages of the Runge-Kutta method [2]. For the Dirichlet boundary conditions, with the time dependent boundary condition $g_1(t)$, the match of time is,

$$\begin{aligned} u^n &\sim g_1(t_n) \\ u^{(1)} &\sim g_1(t_n) + \Delta t g_1'(t_n) \\ u^{(2)} &\sim g_1(t_n) + \frac{1}{2}\Delta t g_1'(t_n) + \frac{1}{4}\Delta t^2 g_1''(t_n) \end{aligned}$$

For the Neumann boundary conditions, with the time dependent boundary condition $g_3(t)$, the match of time is,

$$\begin{aligned} u_x^n &\sim g_3(t_n) \\ u_x^{(1)} &\sim g_3(t_n + \Delta t) \\ u_x^{(2)} &\sim g_3(t_n + \frac{\Delta t}{2}) \end{aligned}$$

2.2 The simplified inverse Lax-Wendroff (SILW) procedure

The basic idea of the SILW procedure is to use Taylor expansion at the boundary point to obtain numerical approximation values at the relevant ghost points. Spatial derivatives at the boundary point can be obtained by two methods: one is repeatedly using the PDE and its time derivatives to convert spatial derivatives to time derivatives,

which are known because of the given boundary conditions, and the other one is the classical extrapolation. The procedure is summarized as follows.

2.2.1 The SILW procedure for Dirichlet boundary conditions

This case corresponds to the IBVP (2.1) with the boundary conditions (2.2).

Assume the inner approximation is a d-th order scheme. Taylor expansion at the boundary points a and b gives

$$u(x_{-p}) = u(a + (C_a - p)\Delta x) = \sum_{k=0}^{d-1} \frac{u_a^{*(k)}(\Delta x)^k(-p + C_a)^k}{k!} + \mathcal{O}(\Delta x^d)$$
$$u(x_{n+p}) = u(b + (p - C_b)\Delta x) = \sum_{k=0}^{d-1} \frac{u_b^{*(k)}(\Delta x)^k(p - C_b)^k}{k!} + \mathcal{O}(\Delta x^d)$$

where $u(x_{-p})$ and $u(x_{n+p})$ are the values of the function u at the ghost points x_{-p} and x_{n+p}, respectively. Clearly,

$$\begin{aligned} u_{-p} &= \sum_{k=0}^{d-1} \frac{u_a^{*(k)}(\Delta x)^k(-p + C_a)^k}{k!} \\ u_{n+p} &= \sum_{k=0}^{d-1} \frac{u_b^{*(k)}(\Delta x)^k(p - C_b)^k}{k!} \end{aligned} \tag{2.7}$$

are d-th order approximations of $u(x_{-p})$ and $u(x_{n+p})$, if $u_a^{*(k)}$ and $u_b^{*(k)}$ are (at least) $(d-k)$-th order approximations of $\frac{\partial^k u}{\partial x^k}|_{x=a}$ and $\frac{\partial^k u}{\partial x^k}|_{x=b}$.

For hyperbolic conservation laws, all the spatial derivatives $u_a^{*(k)}$ and $u_b^{*(k)}$ used in (2.7) can be obtained by the PDE itself and the given boundary condition through the inverse Lax-Wendroff procedure [21, 12] at the inflow boundary. However, in the case of the diffusion equation with Dirichlet boundary conditions, only even order derivatives can be obtained by the PDE itself through this procedure as explained below.

- The even order derivatives can be obtained by the PDE itself through the inverse Lax-Wendroff procedure:

$$u_a^{*(0)} \quad = \quad u(a,t) = g_1(t)$$

$$
\begin{aligned}
u_b^{*(0)} &= u(b,t) = g_2(t) \\
&\cdots \\
u_a^{*(2\beta)} &= \frac{\partial^{(2\beta)} u}{\partial x^{(2\beta)}}|_{x=a} = \frac{1}{c^\beta}\ g_1^{(\beta)}(t) \\
u_b^{*(2\beta)} &= \frac{\partial^{(2\beta)} u}{\partial x^{(2\beta)}}|_{x=b} = \frac{1}{c^\beta}\ g_2^{(\beta)}(t) \\
&\cdots
\end{aligned}
$$

- All derivatives can also be obtained by classical extrapolation.

Assume the d-th order scheme is used in the numerical approximation. We use the following method to obtain the classical interpolation polynomial $P_d(x)$ of degree $d-1$, and then obtain approximations of the derivatives by the corresponding derivatives of $P_d(x)$. We introduce a parameter α between 0 and 1, to distinguish two different ways of obtaining this interpolation polynomial.

1. If $C_a < \alpha$, we use

   $$\{(x_0, u_0),\ (x_1, u_1),\ \cdots,\ (x_{d-1}, u_{d-1})\}$$

   to get the interpolation polynomial $P_{ld}(x)$. Likewise, if $C_b < \alpha$, we use

   $$\{(x_n, u_n),\ (x_{n-1}, u_{n-1}),\ \cdots,\ (x_{n-d+1}, u_{n-d+1})\}$$

   to get the interpolation polynomial $P_{rd}(x)$. We will denote this as *Approach I* below.

2. If $C_a \geq \alpha$, we use

   $$\{(a, g_1(t)),\ (x_0, u_0),\ (x_1, u_1),\ \cdots,\ (x_{d-2}, u_{d-2})\}$$

   to get the interpolation polynomial $P_{ld}(x)$. Likewise, if $C_b \geq \alpha$, we use

   $$\{(b, g_2(t)),\ (x_n, u_n),\ (x_{n-1}, u_{n-1}),\ \cdots,\ (x_{n-d+2}, u_{n-d+2})\}$$

   to get the interpolation polynomial $P_{rd}(x)$. We will denote this as *Approach II* below.

Notice that the difference of these two approaches is whether the boundary datum (e.g. $(a, g_1(t))$) is used in the interpolation polynomial. This datum is not used if the first grid point is too close to the physical boundary (for small α) in *Approach I*, and it is used otherwise in *Approach II*.

Then, for $\beta = 1, 2, \cdots$, we could get approximation to the spatial derivatives at the boundary via extrapolation as

$$\begin{aligned} u_a^{*(\beta)} &= \frac{\partial^{(\beta)} u}{\partial x^{(\beta)}}|_{x=a} = P_{ld}^{(\beta)}(a) \\ u_b^{*(\beta)} &= \frac{\partial^{(\beta)} u}{\partial x^{(\beta)}}|_{x=b} = P_{rd}^{(\beta)}(b). \end{aligned}$$

Our simplified inverse Lax-Wendroff (ILW) procedure is as follows: For $k_d = \bar{k}$ ($1 \leq \bar{k} \leq \frac{d}{2}$), the even derivatives $u_a^{*(2\beta)}$ and $u_b^{*(2\beta)}$, with $\beta = 0, 1, 2 \cdots \bar{k} - 1$ are obtained by the ILW procedure as described above. All remaining derivatives are obtained by extrapolation.

Once we have $u_a^{*(k)}$ and $u_b^{*(k)}$ for all $k = 0, 1, 2 \cdots d-1$, we can plug them into (2.7) to obtain the values at all ghost points x_{-p} and x_{n+p}, thus finishing the boundary treatment.

2.2.2 The SILW procedure for Neumann boundary conditions

This case corresponds to the IBVP (2.1) with the boundary conditions (2.3). The procedure used here is similar to that in Section 2.2.1.

Unlike the d-th order Taylor expansion in equation (2.7), in order to achieve the designed order of accuracy, it seems that a Taylor expansion of order $d + 1$ is needed. Values at the ghost points are approximated as

$$\begin{aligned} u_{-p} &= \sum_{k=0}^{d} \frac{u_a^{*(k)} (\Delta x)^k (-p + C_a)^k}{k!} \\ u_{n+p} &= \sum_{k=0}^{d} \frac{u_b^{*(k)} (\Delta x)^k (p - C_b)^k}{k!} \end{aligned} \tag{2.8}$$

In this case, only the odd order derivatives can be obtained by the boundary data and the PDE itself through the ILW procedure, as explained below.

- The odd order derivatives can be obtained by the PDE itself through the inverse Lax-Wendroff procedure:

$$\begin{aligned} u_a^{*(1)} &= u_x(a,t) = g_3(t) \\ u_b^{*(1)} &= u_x(b,t) = g_4(t) \\ &\cdots \\ u_a^{*(2\beta+1)} &= \frac{\partial^{(2\beta+1)}u}{\partial x^{(2\beta+1)}}|_{x=a} = \frac{1}{c^\beta}\, g_3^{(\beta)}(t) \\ u_b^{*(2\beta+1)} &= \frac{\partial^{(2\beta+1)}u}{\partial x^{(2\beta+1)}}|_{x=b} = \frac{1}{c^\beta}\, g_4^{(\beta)}(t) \\ &\cdots \end{aligned}$$

- All derivatives can also be obtained by classical extrapolation.

Assume the d-th order scheme is used in the numerical approximation. We use the following method to obtain the classical interpolation polynomial $P_{d+1}(x)$ of degree d, and then obtain approximations of the derivatives by the corresponding derivatives of $P_{d+1}(x)$.

1. If $C_a < \alpha$, we use

$$\{(x_0,u_0),\ (x_1,u_1),\ \cdots,\ (x_{d-1},u_{d-1}),\ (x_d,u_d)\}$$

   to get the interpolation polynomial $P_{l(d+1)}(x)$. Likewise, if $C_b < \alpha$, we use

$$\{(x_n,u_n),\ (x_{n-1},u_{n-1}),\ \cdots,\ (x_{n-d+1},u_{n-d+1}),\ (x_{n-d},u_{n-d})\}$$

   to get the interpolation polynomial $P_{r(d+1)}(x)$. We will denote this as *Approach I* below.

2. If $C_a \geq \alpha$, the conditions to determine $P_{l(d+1)}(x)$ are

$$\begin{aligned} P'_{l(d+1)}(a) &= g_3(t) \\ P_{l(d+1)}(x_j) &= u_j,\ j = 0,1,2,\ \cdots,\ d-1. \end{aligned}$$

Likewise, if $C_b \geq \alpha$, the conditions to determine $P_{r(d+1)}(x)$ are

$$\begin{aligned} P'_{r(d+1)}(b) &= g_4(t) \\ P_{r(d+1)}(x_{n-j}) &= u_{n-j},\ j = 0, 1, 2,\ \cdots,\ d-1. \end{aligned}$$

We will denote this as *Approach II* below.

Then, for $\beta = 1, 2, \cdots$, we could get the approximation to the spatial derivatives at the boundary via extrapolation as

$$\begin{aligned} u_a^{*(\beta)} &= \frac{\partial^{(\beta)} u}{\partial x^{(\beta)}}|_{x=a} = P^{(\beta)}_{l(d+1)}(a) \\ u_b^{*(\beta)} &= \frac{\partial^{(\beta)} u}{\partial x^{(\beta)}}|_{x=b} = P^{(\beta)}_{r(d+1)}(b). \end{aligned}$$

Just as before, our simplified inverse Lax-Wendroff (ILW) procedure is as follows: For $k_d = \bar{k}$ $(1 \leq \bar{k} \leq \frac{d}{2})$, the odd order derivatives $u_a^{*(2\beta+1)}$ and $u_b^{*(2\beta+1)}$ with $\beta = 0, 1, 2 \cdots \bar{k} - 1$, are obtained by the ILW procedure as described above. All remaining derivatives needed in equation (2.8) are obtained by extrapolation.

Clearly, the correct choice of the threshold index k_d and the parameter α will be the key issue to ensure stability for both Dirichlet and Neumann boundary conditions. We would like to find the range of α and the minimum threshold index k_d to ensure stability for all $C_a \in [0, 1)$ and $C_b \in [0, 1)$, that is, for all possible relative location of the physical boundary to the closest grid point.

3 Stability analysis

Stability analysis for the semi-discrete schemes and the fully discrete schemes are discussed in this section. Both GKS and eigenvalue spectrum visualization methods are used. For the numerical approximation to the diffusion equation $u_t = cu_{xx}$, the left boundary and the right boundary are completely symmetric for a central scheme. From now on, stability analysis is performed only on the left boundary and we can obtain symmetric conclusions for the right boundary.

3.1 Semi-discrete schemes

In this subsection, we discuss stability of semi-discrete schemes.

3.1.1 The GKS analysis

The key point of the GKS analysis is to find whether there exist eigenvalues or generalized eigenvalues with positive real part. We refer to [12] for a more detailed discussion. If such an eigenvalue and the associated eigensolution exist, the scheme is unstable. Otherwise, the scheme is stable. A detailed description of the procedure for the GKS analysis of semi-discrete schemes can be found in [12] and we omit it here.

• Analysis on Dirichlet boundary conditions

Stability analysis is performed on the left boundary, that is, the right-quarter plane problem

$$\begin{cases} u_t = c\ u_{xx},\ x \in [a, +\infty),\ t \geq 0,\ c > 0 \\ u(a,t) = g_1(t),\ t \geq 0 \\ u(x,0) = u_0(x),\ x \in [a, +\infty) \end{cases} \tag{3.1}$$

For the purpose of stability analysis, $g_1(t)$ can be set to zero without loss of generality.

We take the second order scheme in Section 2.1 as an example to illustrate the analysis procedure. That is,

$$\frac{du_j}{dt} = \frac{c}{\Delta x^2}(u_{j+1} - 2u_j + u_{j-1}), \quad j = 1, 2, \cdots \tag{3.2}$$

Let $u_j = e^{st}\phi_j$, (3.2) can be transformed into

$$\tilde{s}\phi_j = \phi_{j+1} - 2\phi_j + \phi_{j-1} \tag{3.3}$$

Here $\tilde{s} = s\frac{\Delta x^2}{c}$. $\tilde{s}$ can also be regarded as the eigenvalue and $\{\phi_j(\tilde{s})\}_0^\infty$ is the corresponding eigensolution. For the second order scheme, the possible value of k_d is 1.

The characteristic equation is obtained by taking $\phi_j = \kappa^j$ in (3.3):

$$\tilde{s}\kappa = \kappa^2 - 2\kappa + 1 \tag{3.4}$$

Let

$$f(\kappa) = \kappa^2 - (\tilde{s} + 2)\kappa + 1$$

Take $\kappa = e^{\imath\xi}$, $\xi \in [0, 2\pi]$. This means $|\kappa| = 1$. From (3.4), we can get

$$\tilde{s} = e^{\imath\xi} + e^{-\imath\xi} - 2 = 2\cos(\xi) - 2 \tag{3.5}$$

Here, $\tilde{s}$ is real and $\tilde{s} \leq 0$.

Since $x \in [a, +\infty)$, we are only interested in the roots of the characteristic equation which satisfy $|\kappa| < 1$.

As explained in [12], if $Re(\tilde{s}) > 0$, Equation (3.5) also implies that the number of roots with $|\kappa| < 1$ of the characteristic equation is independent of $\tilde{s}$. One can choose any $\tilde{s}$ which satisfies $Re(\tilde{s}) > 0$ to get the number of roots within $|\kappa| < 1$. Taking $\tilde{s} = 1$, the roots of (3.4) are

$$\kappa_1 = 0.381966, \qquad \kappa_2 = 2.61803$$

So, if $Re(\tilde{s}) > 0$, there is just one root satisfying $|\kappa| < 1$.

If $|\kappa| = 1$, which indicates $\tilde{s} \leq 0$, then we are only interested in $\tilde{s} = 0$. The roots of the characteristic equation are $\kappa_1 = \kappa_2 = 1$. A perturbation analysis should be done to decide whether $\kappa = 1$ is stable to perturbation or not. Substituting $\kappa = 1 + \delta$, $\tilde{s} = \varepsilon$ into the characteristic equation (3.4), we obtain $\varepsilon = 1 + \delta + \frac{1}{1+\delta} - 2$. Taylor expansion at $\delta = 0$ gives $\varepsilon = \delta^2 + O(\delta^3)$. If $\varepsilon > 0$, which means that $Re(\tilde{s}) > 0$, $\delta > 0$ or $\delta < 0$. That is, after perturbation, the two roots will satisfy $|\kappa_1| < 1$ and $|\kappa_2| > 1$.

So, if $Re(\tilde{s}) \geq 0$, the two roots of the characteristic equation (3.4) satisfy $|\kappa_1| \leq 1$ and $|\kappa_2| > 1$.

The general expression of ϕ_j in (3.3) is

$$\phi_j = \sigma\kappa^j \tag{3.6}$$

For the SILW boundary treatment, the numerical boundary is (3.2) with $j = 0$ and the values of the ghost points are obtained through the SILW procedure. If $k_d = 1$, the

values of the derivatives are

$$u_a^{*(0)} = u(a,t) = g_1(t) = 0$$

When $\alpha = 1$, only *Approach I* will be used, regardless of the value of C_a. In this case, the points used in the extrapolation are $\{(x_0, u_0),\ (x_1, u_1)\}$, and

$$u_a^{*(1)} = \frac{u_1 - u_0}{\triangle x}$$

When $\alpha = 0$, only *Approach II* will be used, regardless of the value of C_a. In this case, the points used in the extrapolation are $\{(a, 0),\ (x_0, u_0)\}$, and

$$u_a^{*(1)} = \frac{u_0}{C_a \triangle x}$$

By the Taylor expansion (2.7), we can get

$$\begin{cases} u_{-1} = (C_a - 1)(u_1 - u_0), & \text{for } \textit{Approach I} \\ u_{-1} = \dfrac{C_a - 1}{C_a} u_0, & \text{for } \textit{Approach II} \end{cases} \tag{3.7}$$

Plugging (3.6) and (3.7) into the numerical boundary, we can get that

$$\begin{cases} (C_a + 1 - C_a\kappa + \tilde{s})\sigma = 0, & \text{for } \textit{Approach I} \\ (1 + \dfrac{1}{C_a} - \kappa + \tilde{s})\sigma = 0, & \text{for } \textit{Approach II} \end{cases} \tag{3.8}$$

In order to get nontrivial ϕ_j, σ cannot be equal to zero. We need that,

$$\begin{cases} \begin{cases} C_a + 1 - C_a\kappa + \tilde{s} = 0, & \text{for } \textit{Approach I} \\ 1 + \dfrac{1}{C_a} - \kappa + \tilde{s} = 0, & \text{for } \textit{Approach II} \end{cases} \\ f(\kappa) = 0 \\ |\kappa| < 1 \end{cases} \tag{3.9}$$

The method to determine the range of α for stability is as below. First, starting from $\alpha = 0$, then increasing it sequentially with a 0.01 increment, to find $\alpha_{\max}$ which satisfies that, if $C_a \leq \alpha_{\max}$, the scheme with *Approach I* is stable. Next, starting from $\alpha = 1.0$, then decreasing it sequentially with a 0.01 decrement, to find $\alpha_{\min}$ which satisfies that,

if $C_a \geq \alpha_{\min}$, the scheme with *Approach II* is stable. Then the range of α for stability should be $[\alpha_{min}, \alpha_{max}]$.

If we use *Approach II*, there may exist more than one solution to the system (3.9). We compute the largest real part of all the eigenvalues $\tilde{s}$. By using the software Mathematica we get the result as in Fig. 3.1. We notice that the real part of $\tilde{s}$ stays non-positive for all values of C_a.

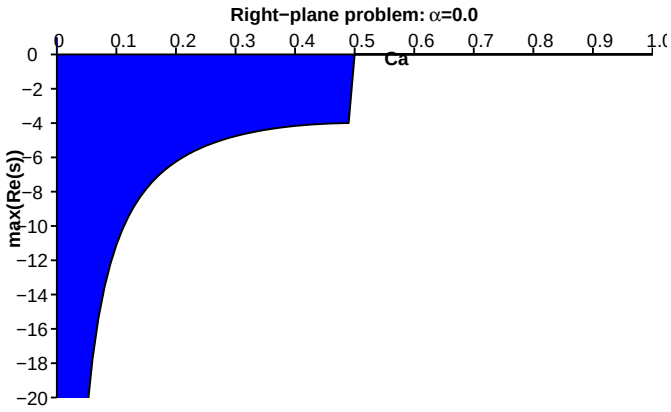

Fig. 3.1. GKS analysis on the right-plane problem: The second order scheme and the SILW procedure with $k_d = 1$ and with *Approach II*.

If we use *Approach I*, the system (3.9) has no solution.

So, for any values of $\alpha \in [0, 1]$, our boundary treatment has no eigenvalue with $Re(\tilde{s}) \geq 0$.

In conclusion, the semi-discrete second order scheme with the SILW procedure with $k_d = 1$ is stable for all values of $C_a \in [0, 1)$, $C_b \in [0, 1)$ and $\alpha \in [0, 1]$.

• Analysis on Neumann boundary conditions

Here, the analysis is performed on the corresponding right-plane problem

$$\begin{cases} u_t = c\, u_{xx},\ x \in [a, +\infty),\ t \geq 0,\ c > 0 \\ u_x(a, t) = g_3(t),\ t \geq 0 \\ u(x, 0) = u_0(x),\ x \in [a, +\infty) \end{cases} \tag{3.10}$$

In order to analyze stability, we set $g_3(t) = 0$ without loss of generality.

For the second order scheme and the SILW procedure with $k_d = 1$, the characteristic equation is (3.4) as in the case of Dirichlet boundary conditions. The eigenvalue problem is (3.3) and the general expression of ϕ_j is (3.6).

In this case, the numerical boundary condition is (3.2) with $j = 0$ and the values of the ghost points are obtained by (2.8).

The value of the first derivative is

$$u_a^{*(1)} = u_x(a,t) = g_3(t) = 0$$

When $\alpha = 1$, only *Approach I* will be used, regardless of the value of C_a. In this case, the points used in the extrapolation are $\{(x_0, u_0),\ (x_1, u_1),\ (x_2, u_2)\}$, and

$$\begin{aligned} u_a^{*(0)} &= \frac{C_a^2 + 3C_a + 2}{2} u_0 - C_a(C_a + 2)u_1 + \frac{C_a(C_a + 1)}{2} u_2 \\ u_a^{*(2)} &= \frac{u_0 - 2u_1 + u_2}{\Delta x^2} \end{aligned}$$

When $\alpha = 0$, only *Approach II* will be used, regardless of the value of C_a. In this case, the constrains to get the interpolation polynomial $P(x)$ are

$$\begin{aligned} P'(a) &= g_3(t) = 0 \\ P(x_j) &= u_j,\ j = 0,\ 1 \end{aligned}$$

In this case,

$$\begin{aligned} u_a^{*(0)} &= \frac{(C_a + 1)^2 u_0 - C_a^2 u_1}{2C_a + 1} \\ u_a^{*(2)} &= \frac{-2u_0 + 2u_1}{(2C_a + 1)\Delta x^2} \end{aligned}$$

By the Taylor expansion (2.8), we can get

$$\begin{cases} u_{-1} = \dfrac{2C_a^2 + C_a + 3}{2} u_0 - (2C_a^2 + 1)u_1 + \dfrac{2C_a^2 - C_a + 1}{2} u_2, & \text{for } \textit{Approach I} \\ u_{-1} = \dfrac{4C_a}{2C_a + 1} u_0 + \dfrac{-2C_a + 1}{2C_a + 1} u_1, & \text{for } \textit{Approach II} \end{cases} \tag{3.11}$$

Plugging (3.6) and (3.11) into the numerical boundary condition, we can get

$$\begin{cases} (\dfrac{2C_a^2 + C_a - 1}{2} - \tilde{s} - 2C_a^2\kappa + \dfrac{2C_a^2 - C_a + 1}{2}\kappa^2)\sigma = 0, & \text{for } \textit{Approach I} \\ (-\dfrac{2}{2C_a + 1} - \tilde{s} + \dfrac{2\kappa}{2C_a + 1})\sigma = 0, & \text{for } \textit{Approach II} \end{cases} \tag{3.12}$$

In order to get nontrivial ϕ_j, σ cannot be equal to zero. We need that,

$$\begin{cases} \begin{cases} \dfrac{2C_a^2 + C_a - 1}{2} - \tilde{s} - 2C_a^2\kappa + \dfrac{2C_a^2 - C_a + 1}{2}\kappa^2 = 0, & \text{for } \textit{Approach I} \\ -\dfrac{2}{2C_a + 1} - \tilde{s} + \dfrac{2\kappa}{2C_a + 1} = 0, & \text{for } \textit{Approach II} \end{cases} \\ f(\kappa) = 0 \\ |\kappa| < 1 \end{cases} \tag{3.13}$$

If we use either *Approach I* or *Approach II*, the system (3.13) has no solution. Therefore, the semi-discrete second order scheme with the SILW procedure with $k_d = 1$ for the Neumann boundary conditions is stable for all $C_a \in [0, 1)$, $C_b \in [0, 1)$ and $\alpha \in [0, 1]$.

3.1.2 Eigenvalue spectrum visualization

Even though the GKS analysis is theoretically sound, it is algebraically very complicated for higher order schemes. We would therefore consider an alternative eigenvalue spectrum visualization method [25], which is less rigorous but is easier to carry out. We will validate our analysis results by numerical experiments in the next section.

The GKS analysis breaks the whole problem into three small problems and by symmetry, we can use the right-quarter problem to get the stability result. Unlike this, the method of eigenvalue spectrum visualization [25] would need to consider stability with the two boundaries together.

In the case of stability analysis, we set $g_1(t) = g_2(t) = 0$ and $g_3(t) = g_4(t) = 0$ without loss of generality.

The semi-discrete schemes can be expressed as a linear system of equations in a matrix-vector form as

$$\frac{d\vec{U}}{dt} = \frac{c}{\Delta x^2} Q\vec{U} \tag{3.14}$$

where $\vec{U} = (u_0,\ u_1,\ \cdots,\ u_N)^T$ and Q is the coefficient matrix of the spatial discretization. This system contains the chosen inner scheme as well as two numerical boundary conditions.

Let $u(x,t) = e^{st}v(x)$, (3.14) changes to

$$\tilde{s}\vec{U} = Q\vec{U} \tag{3.15}$$

As pointed out in [25], we only need to focus on the eigenvalues which both keep $O(1)$ distance from the imaginary axis when the grid number N increases and satisfy $Re(\tilde{s}) > 0$. Therefore, we look for "fixed" eigenvalues, namely those eigenvalues which are equal (subject to a negligible difference due to round-off errors and eigenvalue solver accuracy) for different values of the grid number N. Just like in the GKS analysis, there may be more than one such fixed eigenvalues of the matrix Q, and we are mostly interested in the largest real part of all such eigenvalues. We perform this analysis with the second order scheme with the SILW procedure with $k_d = 1$ as an example, using Matlab.

Similar to the analysis in Section 3.1.1, we only perform the analysis on the right-quarter plane problem. But in order to obtain the matrix form (3.14), we would need a finite interval. In our second order scheme, numerical boundaries are still given by the inner scheme (3.2) with $j = 0$ and $j = N$, with the ghost point values at x_{-1} and x_{N+1} determined by the boundary procedure: u_{-1} is obtained by the SILW procedure in the the GKS analysis, and we set $u_{N+1} = 0$ to eliminate the influence to stability from the right boundary.

• Dirichlet boundary conditions

If we use *Approach II*, the largest real part of all the fixed eigenvalues is shown in Fig. 3.2, in which we have used three different values of N ($N = 320$, 640 and 1280) to find the largest real part of all fixed eigenvalues which do not get closer to the imaginary axis when N increases over this range.

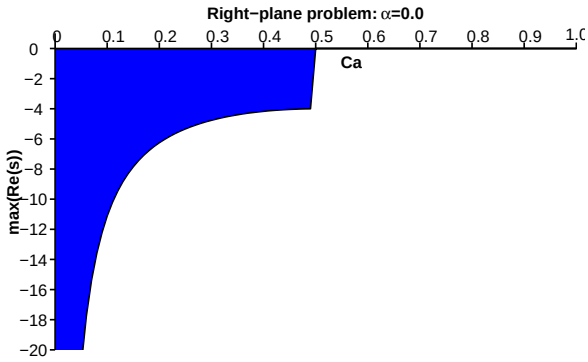

Fig. 3.2. Eigenvalue spectrum visualization on the right-plane problem: The second order scheme with the SILW procedure with $k_d = 1$ and using *Approach II*.

If we use *Approach I*, there is no fixed eigenvalue for any $C_a \in [0, 1)$.

This leads us to the same conclusion that the semi-discrete second order approximation scheme with the SILW procedure with $k_d = 1$ is stable for all values of $C_a \in [0, 1)$, $C_b \in [0, 1)$ and $\alpha \in [0, 1]$.

Comparing Figs. 3.1 and 3.2, we find that they are almost the same. So we have confidence that the eigenvalue spectrum visualization method is reliable.

• Neumann boundary conditions

In this case, there is no fixed eigenvalue for all $C_a \in [0, 1)$ either with *Approach I* or with *Approach II* as boundary conditions.

3.2 Fully discrete schemes

In this paper, the third order TVD Runge-Kutta time discretization is used. Detailed description can be found in [12] and we will just briefly describe this method here.

In the semi-discrete case, an eigensolution is in the form $u_j(t) = e^{st}\phi_j = e^{\tilde{s}c\frac{t}{\Delta x^2}}\phi_j$ with $Re(\tilde{s}) \geq 0$. In the fully-discrete scheme, an eigensolution is in the form $u_j^{n+1} = z(\mu)u_j^n$ with $\mu = s\Delta t = \tilde{s}\frac{c\Delta t}{\Delta x^2}$ and $|z(\mu)| > 1$ where

$$z(\mu) = 1 + \mu + \frac{\mu^2}{2} + \frac{\mu^3}{6} \tag{3.16}$$

Here, $\tilde{s}$ is an eigenvalue of the semi-discrete scheme. In both semi-discrete and fully

discrete cases, the scheme is unstable if such candidate eigensolution exists. Take

$$\lambda_{cfl} = \frac{c\Delta t}{\Delta x^2}$$

where $\lambda_{cfl} > 0$. From now on, we would like to verify stability with $(\lambda_{cfl})_{\max}$, which is the maximum value of λ_{cfl} to ensure stability for the corresponding Cauchy problem of the inner scheme without boundary. In other words, we would not want the boundary condition to reduce the CFL number for stability. The details of the method to get $(\lambda_{cfl})_{\max}$ can be found in [12] and we just list the values of $(\lambda_{cfl})_{\max}$ for schemes in this paper in Table 3.1.

Table 3.1. $(\lambda_{cfl})_{\max}$ for the schemes of different orders

Scheme	2^{nd} order	4^{th} order	6^{th} order	8^{th} order	10^{th} order
$(\lambda_{cfl})_{max}$	0.628	0.471	0.415	0.386	0.368

3.2.1 The GKS analysis

For the GKS analysis, $\tilde{s}$ is the eigenvalue obtained in the semi-discrete case and

$$\mu = s\Delta t = (\lambda_{cfl})_{\max}\tilde{s}$$

• Dirichlet boundary conditions

Take $\alpha = 0$, namely we use *Approach II* as the boundary condition. There may exist more than one eigenvalues $\tilde{s}$, the maximum value of $|z(\mu)|$ as defined in equation (3.16) is shown in Fig. 3.3 by the software Mathematica.

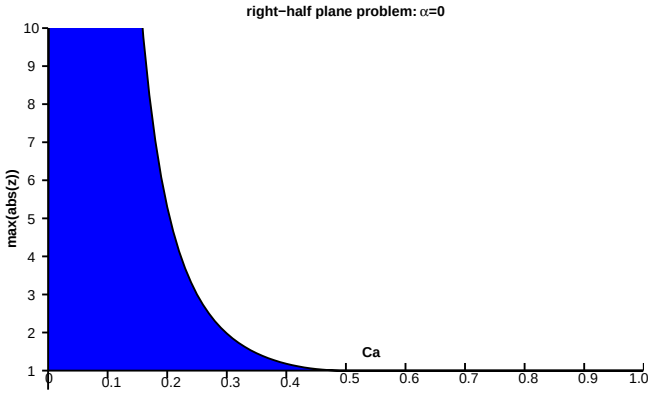

Fig. 3.3. GKS analysis on the right-plane problem: The second order scheme with the SILW procedure with $k_d = 1$ and using *Approach II*.

As in the semi-discrete case, if $\alpha = 1.0$, namely if we use *Approach I* as the boundary condition, there exists no eigenvalue and the scheme is stable for all $C_a \in [0, 1)$.

• Neumann boundary conditions

As the semi-discrete case, whether we use *Approach I* or *Approach II* as boundary conditions, there exists no eigenvalue and the scheme is stable for all $C_a \in [0, 1)$.

3.2.2 Eigenvalue spectrum visualization

In this subsection, we give the results of the Dirichlet boundary conditions using the eigenvalue spectrum visualization. This method is based on the matrix formulation (3.14).

As is the same procedure in [12], we need all the eigenvalues of

$$G = I + \frac{c\Delta t}{\Delta x^2}Q + \frac{1}{2}(\frac{c\Delta t}{\Delta x^2}Q)^2 + \frac{1}{6}(\frac{c\Delta t}{\Delta x^2}Q)^3$$

to lie inside the unit circle. i.e. $|z(\mu)| \leq 1$, to ensure stability of the fully discrete approximation. Here I is the identity matrix.

The result of the second order scheme with the SILW procedure with $k_d = 1$ and using *Approach II* as boundary condition is shown in Fig. 3.4.

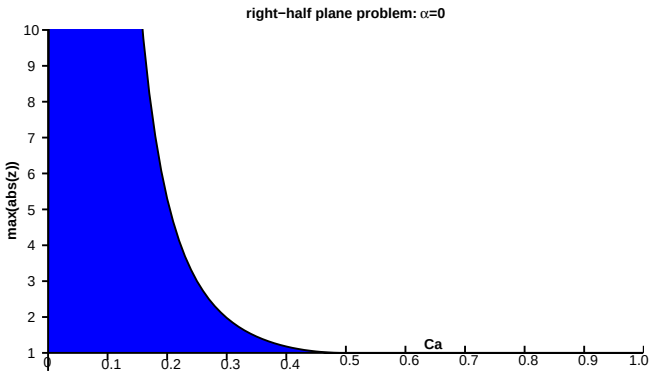

Fig. 3.4. Eigenvalue spectrum visualization on the right-plane problem: The second order scheme with the SILW procedure with $k_d = 1$ and using *Approach II*.

If we use *Approach I* as the boundary condition, there is no fixed eigenvalue of G and the fully-discrete scheme is stable for all C_a.

We notice that Figs. 3.3 and 3.4 are almost identical. From these two figures, we can find that if we take $\alpha < 0.5$, the SILW procedure with $k_d = 1$ cannot guarantee stability for all C_a and C_b in the fully discrete case. If take $\alpha \geq 0.5$, the scheme is stable.

In conclusion, in order to ensure stability of the second order fully discrete scheme with the SILW procedure with $k_d = 1$ for all C_a and C_b, the value of α should satisfy $\alpha \in [0.5, 1.0]$.

For the remaining schemes in Section 2.1, we have performed similar analysis. Results as in Fig. 3.4 for the fourth order scheme are shown in Figs. 3.5–3.6. Results for higher order schemes are not shown in figures in order to save space. We summarize the results of the analysis for the ranges of α to ensure stability in Table 3.2.

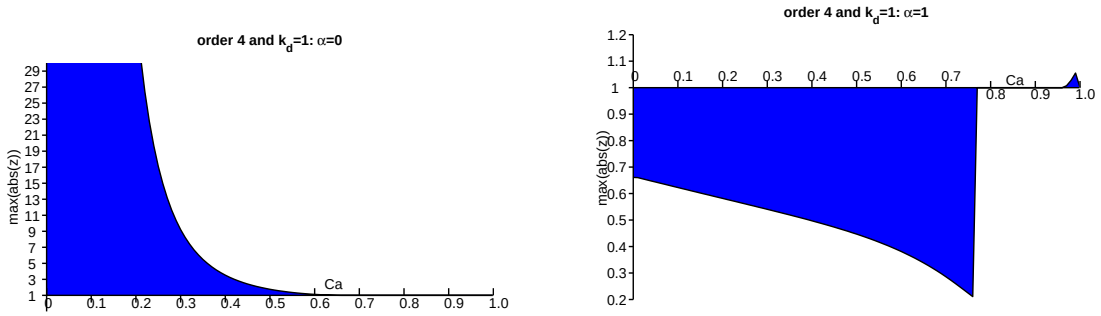

Fig. 3.5. The fourth order scheme with the SILW procedure with $k_d = 1$ on the right-quarter problem (3.1). Left: $\alpha = 0.0$ (using *Approach II*); Right: $\alpha = 1.0$ (using *Approach I*).

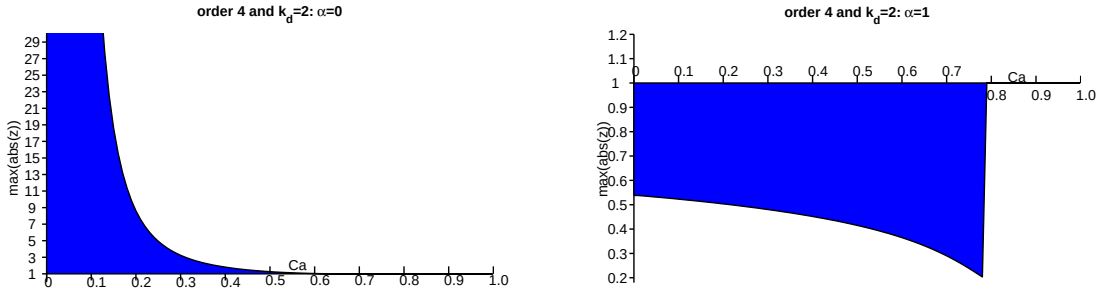

Fig. 3.6. The fourth order scheme with the SILW procedure with $k_d = 2$ on the right-quarter problem (3.1). Left: $\alpha = 0.0$ (using *Approach II*); Right: $\alpha = 1.0$ (using *Approach I*).

Table 3.2. The range of α to ensure stability for schemes of different orders for the IBVP (2.1) with Dirichlet boundary conditions (2.2).

Scheme	2^{nd} order	4^{th} order	6^{th} order	8^{th} order	10^{th} order
$k_d = 1$	[0.5, 1.0]	[0.67, 0.96]	[0.59, 0.83]	–	–
$k_d = 2$	–	[0.65, 0.99]	[0.52, 0.90]	[0.33, 0.85]	[0.27, 0.83]
$k_d = 3$	–	–	[0.61, 0.90]	[0.51, 0.85]	[0.47, 0.82]
$k_d = 4$	–	–	–	[0.49, 0.85]	[0.41, 0.82]
$k_d = 5$	–	–	–	–	[0.41, 0.82]

In Table 3.2, we summarize the results of the stability analysis, giving the range of α required for the SILW boundary treatment for schemes of different orders of accuracy to remain stable for the IBVP (2.1) with the Dirichlet boundary conditions (2.2), under the same $(\lambda_{cfl})_{\max}$ as shown in Table 3.1 for pure initial value problems. Again, the third order TVD Runge-Kutta method is used for the time discretization. In practice, we would recommend using the middle value of the stability range of α in each case.

We note that the eighth order scheme with $k_d = 1$ is unstable if $C_a \leq 0.02$ or $C_b \leq 0.02$. The tenth order scheme with $k_d = 1$ is unstable if $C_a \leq 0.20$ or $C_b \leq 0.20$. Hence, in these two cases, there exists no α to ensure stability for every C_a and C_b with the SILW procedure with $k_d = 1$, and we need to take at least $k_d = 2$ in the SILW procedure.

3.2.3 Results for Neumann boundary conditions

As for the semi-discrete case, the fully discrete second order scheme with Neumann boundary conditions using the SILW procedure with $k_d = 1$ has no fixed eigenvalue for either $\alpha = 0$ (using *Approach II* as the boundary treatment) or $\alpha = 1.0$ (using *Approach I* as the boundary treatment).

The results for the fourth order scheme in Section 2.1 with the Neumann boundary conditions (2.3) and the SILW procedure introduced in Section 2.2.2 are shown in Figs. 3.7–3.8. Similar results for higher order schemes are not shown in figures to save space. We summarize the results of analysis for the ranges of α to ensure stability in Table 3.3.

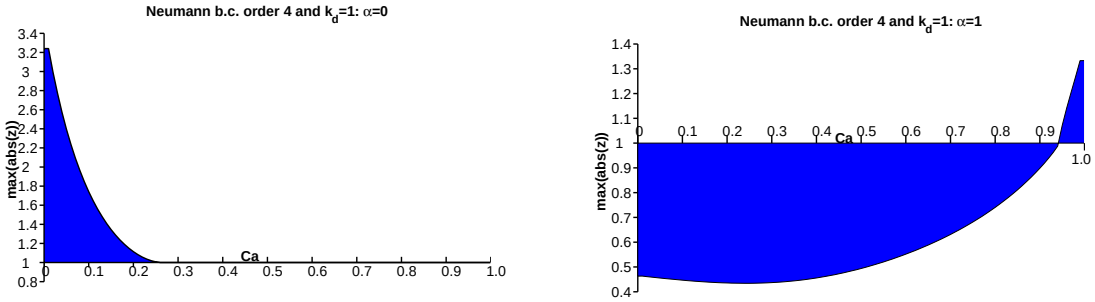

Fig. 3.7. The fourth order scheme using the SILW procedure with $k_d = 1$ on the right-quarter problem (3.10). Left: $\alpha = 0.0$ (with *Approach II*); Right: $\alpha = 1.0$ (with *Approach I*).

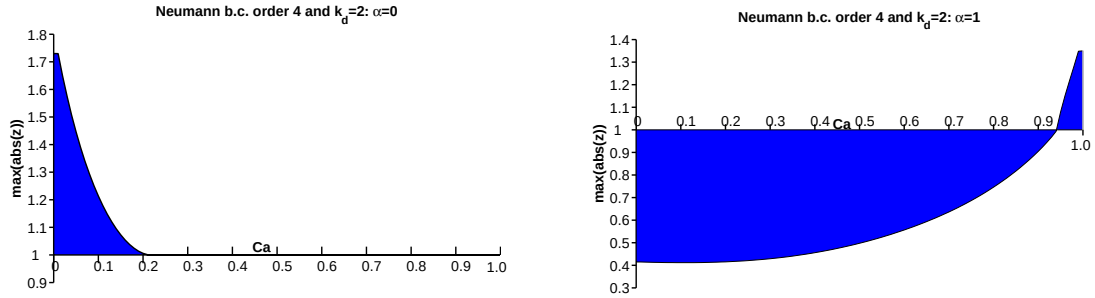

Fig. 3.8. The fourth order scheme using the SILW procedure with $k_d = 2$ on the right-quarter problem (3.10). Left: $\alpha = 0.0$ (with *Approach II*); Right: $\alpha = 1.0$ (with *Approach I*).

Table 3.3. The range of α to ensure stability for the schemes of different orders of accuracy for the IBVP (2.1) with the Neumann boundary condition (2.3).

Scheme	2^{nd} order	4^{th} order	6^{th} order	8^{th} order	10^{th} order
$k_d = 1$	[0, 0.99]	[0.27, 0.94]	[0.25, 0.90]	[0.20, 0.86]	[0.17, 0.84]
$k_d = 2$	–	[0.22, 0.94]	[0.21, 0.88]	[0.12, 0.82]	[0.07, 0.76]
$k_d = 3$	–	–	[0.24, 0.88]	[0.22, 0.82]	[0.21, 0.77]
$k_d = 4$	–	–	–	[0.21, 0.82]	[0.17, 0.77]
$k_d = 5$	–	–	–	–	[0.18, 0.77]

In Table 3.3, we summarize the results of the stability analysis, giving the range of α required for the SILW boundary treatment for different schemes to remain stable for the IBVP (2.1) with the Neumann boundary condition (2.3), under the same $(\lambda_{cfl})_{\max}$ as shown in Table 3.1 for pure initial value problems. Again, the third order TVD Runge-Kutta method is used for the time discretization. We can see from this table that in this case, the SILW boundary treatment with $k_d = 1$ can ensure stability for all schemes up to order 10 within certain ranges of α. In practice, we again recommend to use the the middle value of the stability range of α in each case.

Results in Tables 3.2 and 3.3 for high order schemes are obtained by the eigenvalue spectrum visualization method experimentally. Even though there is no rigorous proof for this method, it can produce similar results as the GKS analysis when both are applied, as indicated before. The numerical results in Section 4 also validate the results obtained through the spectrum visualization method numerically.

4 Numerical examples

In this subsection, numerical tests are performed to illustrate and validate the results in Sections 3.2.2 and 3.2.3.

4.1 Example 1

In this section, we provide numerical examples to demonstrate the stability results predicted by the analysis in Tables 3.2 and 3.3.

The example is

$$\begin{cases} u_t = \ u_{xx}, \ x \in [\frac{1}{2}, 1], \ t \geq 0 \\ \textit{boundary conditions} \\ u(x,0) = \sin(x), \ x \in [\frac{1}{2}, 1] \end{cases} \tag{4.1}$$

The corresponding Dirichlet boundary conditions are

$$\begin{cases} u(\frac{1}{2},t) = e^{-t}\sin(\frac{1}{2}) \\ u(1,t) = e^{-t}\sin(1) \end{cases} \tag{4.2}$$

The corresponding Neumann boundary conditions are

$$\begin{cases} u_x(\frac{1}{2},t) = e^{-t}\cos(\frac{1}{2}) \\ u_x(1,t) = e^{-t}\cos(1) \end{cases} \tag{4.3}$$

The exact solution is

$$u(x,t) = e^{-t}\sin(x)$$

The time step size Δt is chosen as

$$\Delta t = (\lambda_{cfl})_{\max}\Delta x^2 \tag{4.4}$$

where $(\lambda_{cfl})_{\max}$ is the maximum CFL number shown in Table 3.1 for stability of pure initial value problems.

4.1.1 Results for Dirichlet boundary conditions

In this subsection, we give the results of equation (4.1) with the boundary condition (4.2).

• The second order scheme

Fig. 4.1 (left) shows that the solution has strong spurious oscillations with very large magnitudes, when we use $\alpha = 0.49$ with only $N = 40$ grid points. This clearly demonstrates that the method is unstable. If we take $\alpha = 0.50$, as shown in Fig. 4.1 (right), the solution remains stable and accurate after a grid refinement. These results are perfectly consistent with the analysis before. From Tables 4.1 and 4.2, a grid refinement study verifies the designed second order accuracy when the scheme is stable.

Table 4.1. The second order scheme with $k_d = 1$, $\alpha = 0.75$, $t_{end} = 1.0$ for (4.1) and (4.2).

N	$C_a = 0.99999,\ C_b = 0.99999$				$C_a = 0.749,\ C_b = 0.751$			
	L^2 *error*	order	L^∞ *error*	order	L^2 *error*	order	L^∞ *error*	order
10	2.333E-05	–	5.724E-05	–	6.371E-05	–	1.172E-04	–
20	7.450E-06	1.647	1.806E-05	1.664	1.815E-05	1.811	3.327E-05	1.817
40	2.121E-06	1.813	5.059E-06	1.836	4.860E-06	1.901	8.885E-06	1.905
80	5.698E-07	1.896	1.515E-06	1.739	1.258E-06	1.949	2.297E-06	1.951
160	1.471E-07	1.953	3.621E-07	2.065	3.202E-07	1.974	5.841E-07	1.975

Table 4.2. The second order scheme with $k_d = 1$, $\alpha = 1.0$, $t_{end} = 1.0$ for (4.1) and (4.2).

N	$C_a = 10^{-6},\ C_b = 10^{-6}$				$C_a = 0.99999,\ C_b = 0.99999$			
	L^2 *error*	order	L^∞ *error*	order	L^2 *error*	order	L^∞ *error*	order
10	4.677E-04	–	7.758E-04	–	6.017E-07	–	1.165E-06	–
20	1.140E-04	2.036	1.936E-04	2.003	1.790E-07	1.749	3.465E-07	1.749
40	2.815E-05	2.018	4.838E-05	2.001	4.911E-08	1.866	9.525E-08	1.863
80	6.993E-06	2.009	1.209E-05	2.000	1.288E-08	1.930	2.499E-08	1.931
160	1.743E-06	2.005	3.023E-06	2.000	3.301E-09	1.965	6.402E-09	1.965

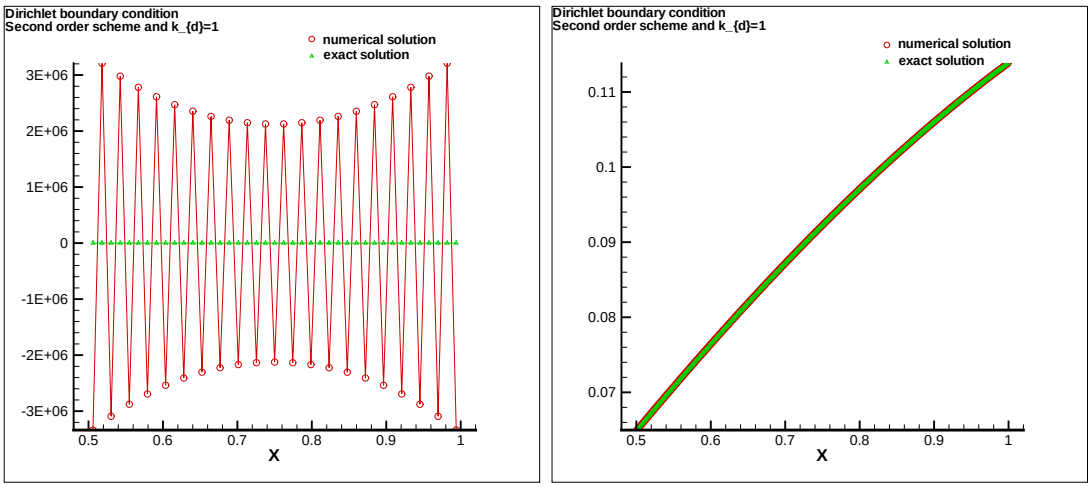

Fig. 4.1. Numerical results for (4.1) and (4.2) obtained with the second order scheme using the SILW procedure with $k_d = 1$. $C_a = C_b = 0.49$. $t_{end} = 2.0$. Left: $\alpha = 0.49$ with $N = 40$ grid points; Right: $\alpha = 0.50$ with $N = 320$ grid points.

- The fourth order scheme

We will only explore the case with $k_d = 1$. Figs. 4.2 (left) and 4.3 (left) show that, when $\alpha = 0.66$ and $\alpha = 0.97$ respectively, the solution has strong spurious oscillations

with very large magnitudes when only $N = 20$ grid points are used. This clearly demonstrates that the method is unstable. As shown in Figs. 4.2 (right) and 4.3 (right), when $\alpha = 0.67$ and $\alpha = 0.96$ respectively, the solution remains stable and accurate after a grid refinement. These results are consistent with the analysis before. From Table 4.3, a grid refinement study verifies the designed fourth order accuracy when the scheme is stable.

Table 4.3. The fourth order scheme with $k_d = 1$, $\alpha = 0.82$, $t_{end} = 1.0$ for (4.1) and (4.2).

N	$C_a = 10^{-6}$, $C_b = 0.99999$				$C_a = 0.819$, $C_b = 0.821$			
	L^2 *error*	order	L^∞ *error*	order	L^2 *error*	order	L^∞ *error*	order
10	2.497E-07	–	6.257E-07	–	1.409E-08	–	3.229E-08	–
20	1.732E-08	3.849	4.530E-08	3.788	1.211E-09	3.539	3.016E-09	3.420
40	1.139E-09	3.972	3.051E-09	3.892	9.009E-11	3.749	2.356E-10	3.678
80	7.300E-11	3.964	1.979E-10	3.946	6.167E-12	3.869	1.649E-11	3.837
160	4.593E-12	3.990	1.261E-11	3.973	3.790E-13	4.024	1.088E-12	3.921

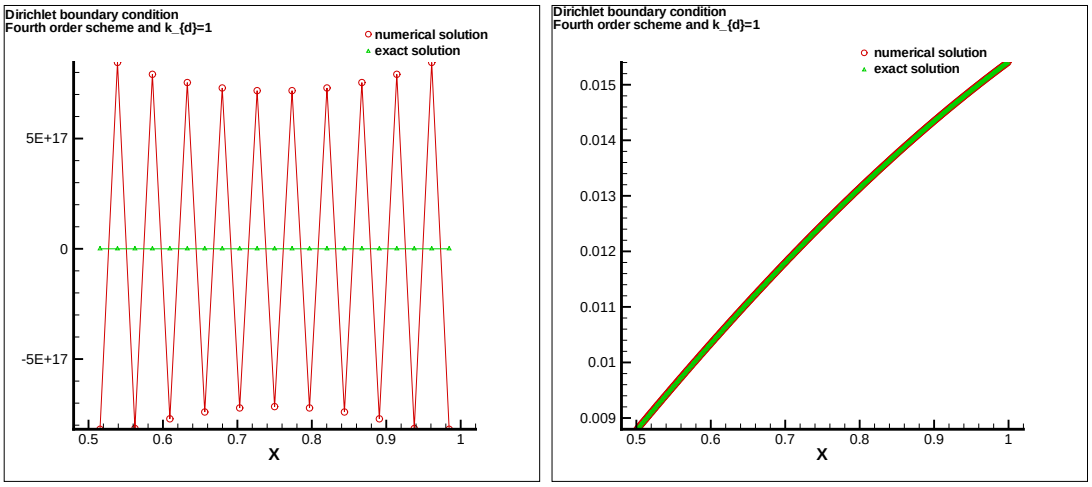

Fig. 4.2. Numerical results for (4.1) and (4.2) obtained with the fourth order scheme using the SILW procedure with $k_d = 1$. $C_a = C_b = 0.66$. $t_{end} = 4.0$. Left: $\alpha = 0.66$ with $N = 20$ grid points; Right: $\alpha = 0.67$ with $N = 320$ grid points.

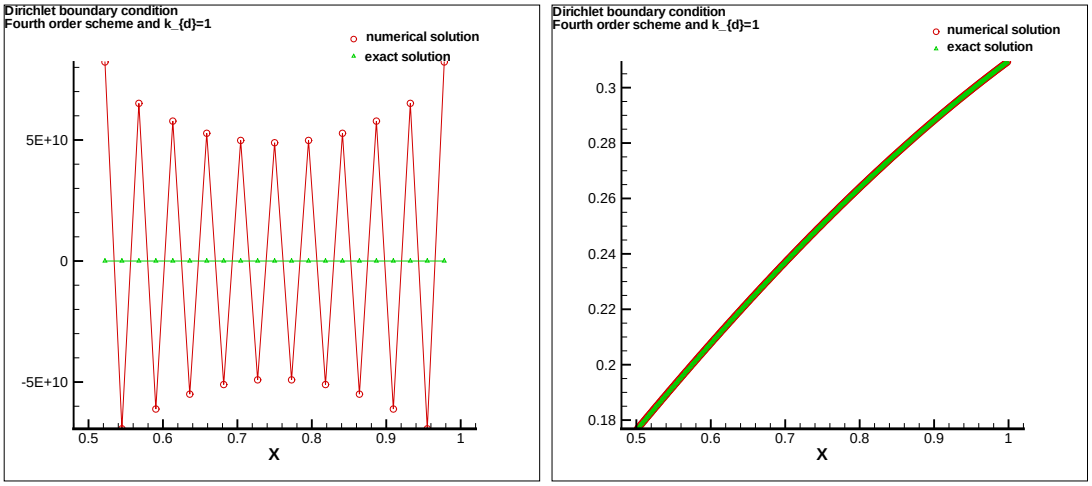

Fig. 4.3. Numerical results for (4.1) and (4.2) obtained with the fourth order scheme using the SILW procedure with $k_d = 1$. $C_a = C_b = 0.969$. $t_{end} = 1.0$. Left: $\alpha = 0.97$ with $N = 20$ grid points; Right: $\alpha = 0.96$ with $N = 320$ grid points.

We have also performed numerical tests for the case with $k_d = 2$, obtaining again results perfectly consistent with the analysis before. We will not present the results here to save space.

For the remaining sixth order, eighth order and tenth order schemes, we will only display results of the minimum value of k_d which yields stability. For the other cases, we have performed the analysis and obtained results which are consistent with the analysis, but we will omit them to save space.

• The sixth order scheme

In this case, the minimum value of k_d is 1. Figs. 4.4 (left) and 4.5 (left) clearly show instability. When α is in the appropriate interval, the scheme becomes stable as shown in Figs. 4.4 (right) and 4.5 (right), which is consistent with the analysis.

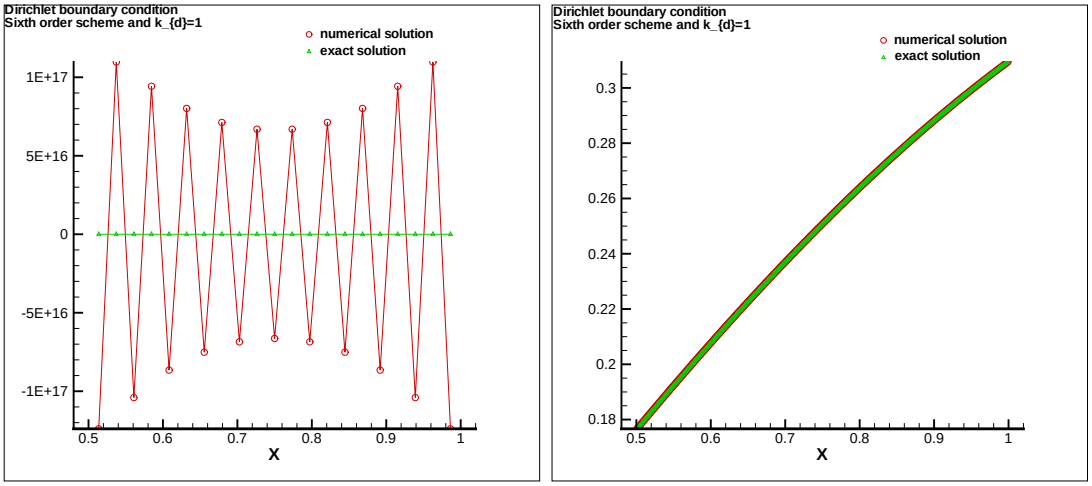

Fig. 4.4. Numerical results for (4.1) and (4.2) obtained with the sixth order scheme and the SILW procedure with $k_d = 1$. $C_a = C_b = 0.58$ with $t_{end} = 1.0$. Left: $\alpha = 0.58$ with $N = 20$ grid points; Right: $\alpha = 0.59$ with $N = 320$ grid points.

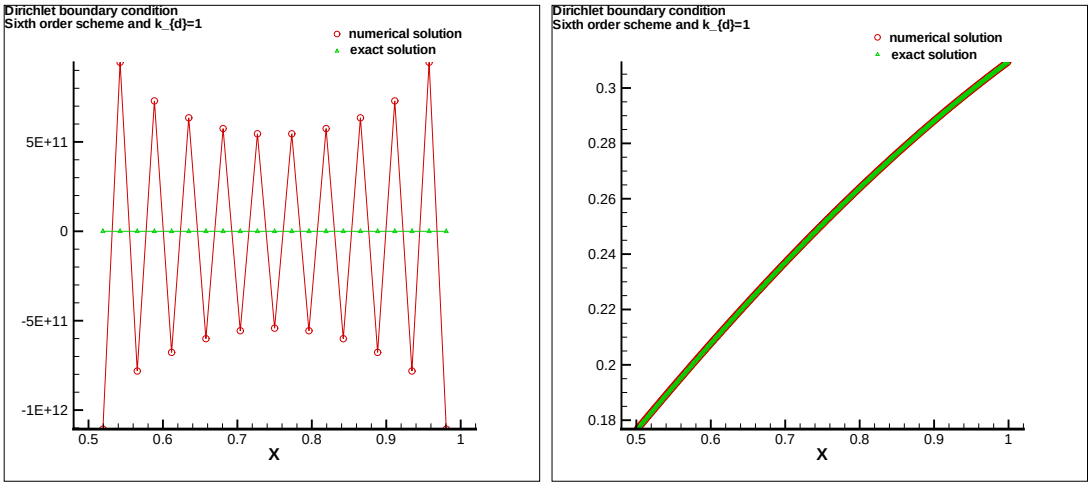

Fig. 4.5. Numerical results for (4.1) and (4.2) obtained with the sixth order scheme and the SILW procedure with $k_d = 1$. $C_a = C_b = 0.839$ with $t_{end} = 1.0$. Left: $\alpha = 0.84$ with $N = 20$ grid points; Right: $\alpha = 0.83$ with $N = 320$ grid points.

- The eighth order scheme

In this case, the minimum value of k_d is 2. Figs. 4.6 (left) and 4.7 (left) clearly show instability. Figs. 4.6 (right) and 4.7 (right) show stability with appropriate choices of α.

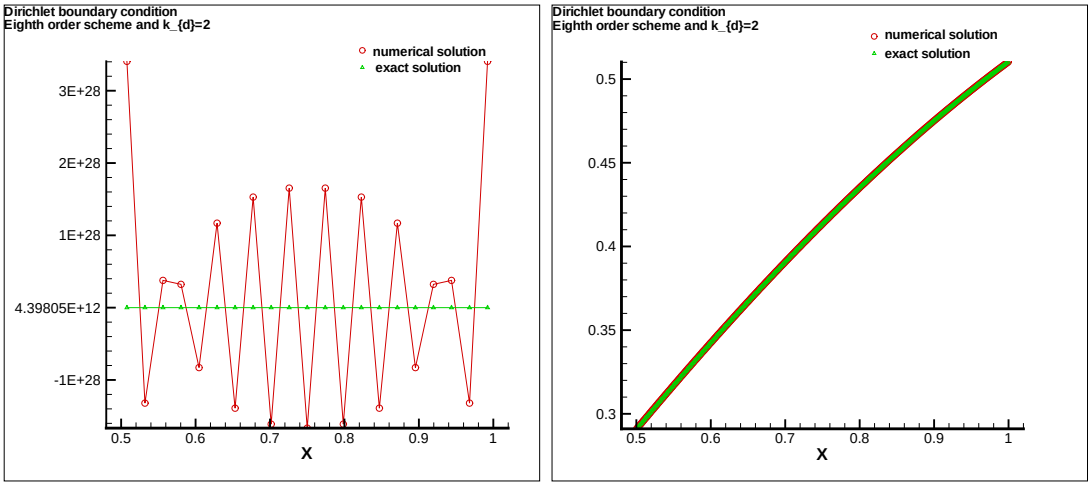

Fig. 4.6. Numerical results for (4.1) and (4.2) obtained with the eighth order scheme and the SILW procedure with $k_d = 2$. $C_a = C_b = 0.32$ with $t_{end} = 0.5$. Left: $\alpha = 0.32$ with $N = 20$ grid points; Right: $\alpha = 0.33$ with $N = 320$ grid points.

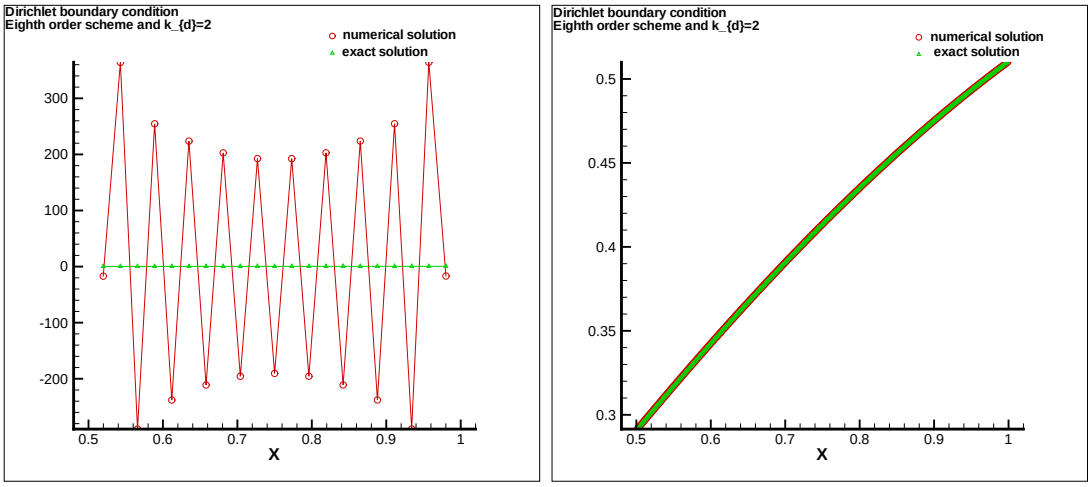

Fig. 4.7. Numerical results for (4.1) and (4.2) obtained with the eighth order scheme and the SILW procedure with $k_d = 2$. $C_a = C_b = 0.8599$ with $t_{end} = 0.5$. Left: $\alpha = 0.86$ with $N = 20$ grid points; Right: $\alpha = 0.85$ with $N = 320$ grid points.

- The tenth order scheme

The simulation is repeated for the tenth order scheme. In this case, the minimum value of k_d is 2. Figs. 4.8 (left) and 4.9 (left) clearly show instability. Figs. 4.8 (right) and 4.9 (right) show stability. These results are consistent with the analysis.

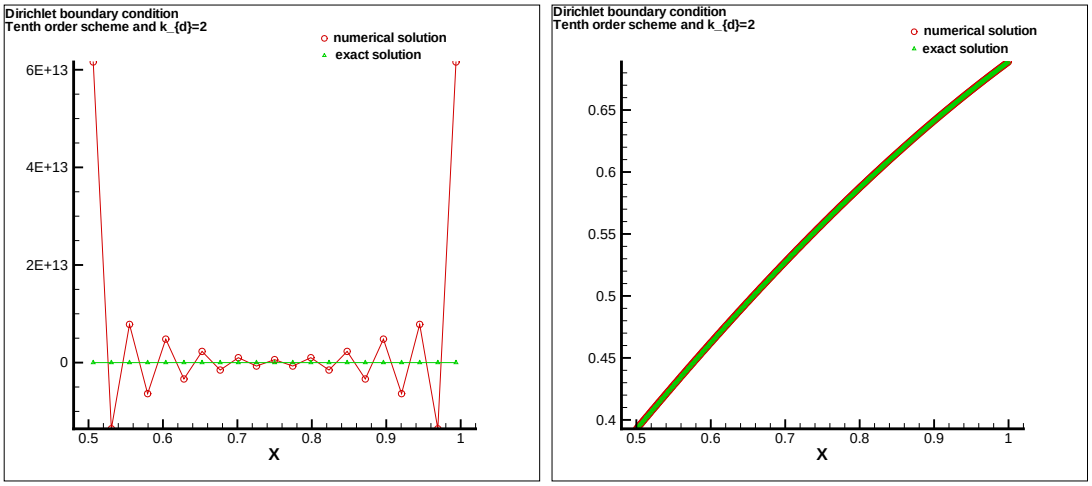

Fig. 4.8. Numerical results for (4.1) and (4.2) obtained with the tenth order scheme and the SILW procedure with $k_d = 2$. $C_a = C_b = 0.26$ with $t_{end} = 0.2$. Left: $\alpha = 0.26$ with $N = 20$ grid points; Right: $\alpha = 0.27$ with $N = 320$ grid points.

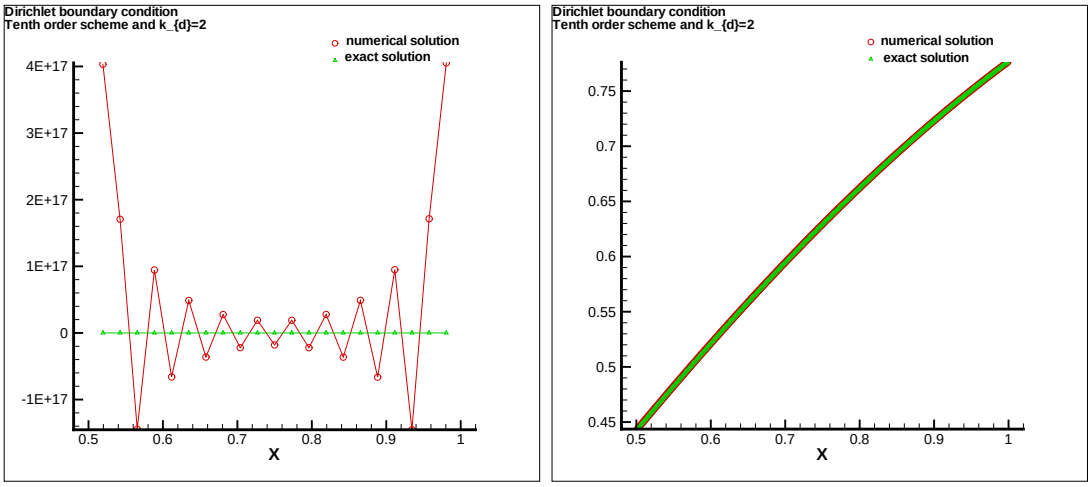

Fig. 4.9. Numerical results for (4.1) and (4.2) obtained with the tenth order scheme and the SILW procedure with $k_d = 2$. $C_a = C_b = 0.839$ with $t_{end} = 0.08$. Left: $\alpha = 0.84$ with $N = 20$ grid points; Right: $\alpha = 0.83$ with $N = 320$ grid points.

4.1.2 Results for Neumann boundary conditions

- The second order scheme

From Tables 4.4 and 4.5, we can find that the scheme, when it is stable, can reach the desired second order accuracy. Comparison of stability and instability results are given in Fig. 4.10.

Table 4.4. The second order scheme with $k_d = 1$, $\alpha = 0$, $t_{end} = 1.0$ for (4.1) and (4.3).

N	$C_a = 10^{-6}$, $C_b = 10^{-6}$				$C_a = 0.99999$, $C_b = 0.99999$			
	L^2 *error*	order	L^∞ *error*	order	L^2 *error*	order	L^∞ *error*	order
10	6.735E-05	–	1.191E-04	–	1.887E-04	–	3.119E-04	–
20	1.641E-05	2.037	2.976E-05	2.001	6.015E-05	1.650	9.791E-05	1.672
40	4.047E-06	2.019	7.440E-06	2.000	1.714E-05	1.811	2.767E-05	1.823
80	1.005E-06	2.010	1.860E-06	2.000	4.587E-06	1.902	7.372E-06	1.908
160	2.503E-07	2.005	4.650E-07	2.000	1.187E-06	1.950	1.904E-06	1.953

Table 4.5. The second order scheme with $k_d = 1$, $\alpha = 0.5$, $t_{end} = 1.0$ for (4.1) and (4.3).

N	$C_a = 10^{-6}$, $C_b = 0.99999$				$C_a = 0.501$, $C_b = 0.499$			
	L^2 *error*	order	L^∞ *error*	order	L^2 *error*	order	L^∞ *error*	order
10	1.371E-03	–	1.997E-03	–	1.091E-03	–	1.612E-03	–
20	3.749E-04	1.870	5.470E-04	1.868	2.905E-04	1.908	4.306E-04	1.904
40	9.819E-05	1.933	1.434E-04	1.932	7.495E-05	1.955	1.113E-04	1.952
80	2.513E-05	1.966	3.671E-05	1.965	1.903E-05	1.977	2.828E-05	1.976
160	6.358E-06	1.983	9.288E-06	1.983	4.796E-06	1.989	7.128E-06	1.988

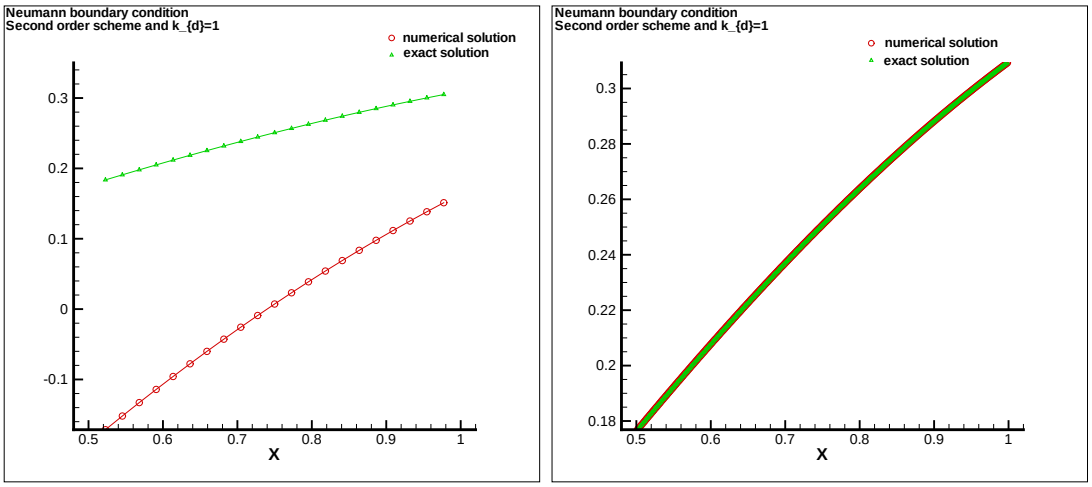

Fig. 4.10. Numerical results for (4.1) and (4.3) obtained with the second order scheme and the SILW procedure with $k_d = 1$. $C_a = C_b = 0.99999$ with $t_{end} = 1.0$. Left: $\alpha = 1.0$ with $N = 20$ grid points; Right: $\alpha = 0.99$ with $N = 320$ grid points.

- The fourth order scheme

As before, we will only explore the case with $k_d = 1$. Figs. 4.11 and 4.12 show the stability-instability results. From Table 4.6 we can find that the scheme is stable for

$\alpha = 0.60$ and we can also obtain the desired fourth order accuracy.

Table 4.6. The fourth order scheme with $k_d = 1$, $\alpha = 0.6$, $t_{end} = 1.0$ for (4.1) and (4.3).

N	$C_a = 10^{-6}$, $C_b = 0.99999$				$C_a = 0.599$ and $C_b = 0.601$			
	L^2 *error*	order	L^∞ *error*	order	L^2 *error*	order	L^∞ *error*	order
10	2.572E-06	–	3.720E-06	–	2.924E-06	–	4.329E-06	–
20	1.931E-07	3.735	2.797E-07	3.733	2.351E-07	3.637	3.477E-07	3.638
40	1.327E-08	3.864	1.923E-08	3.863	1.675E-08	3.811	2.475E-08	3.812
80	8.696E-10	3.931	1.261E-09	3.931	1.119E-09	3.904	1.653E-09	3.904
160	5.627E-11	3.950	8.158E-11	3.950	7.178E-11	3.962	1.061E-10	3.962

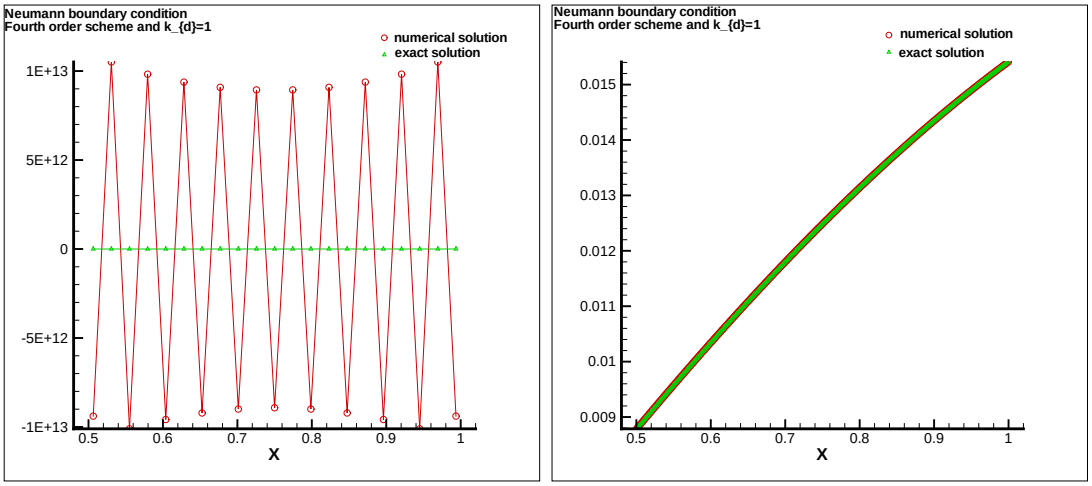

Fig. 4.11. Numerical results for (4.1) and (4.3) obtained with the fourth order scheme and the SILW procedure with $k_d = 1$. $C_a = C_b = 0.26$ with $t_{end} = 4.0$. Left: $\alpha = 0.26$ with $N = 20$ grid points; Right: $\alpha = 0.27$ with $N = 320$ grid points.

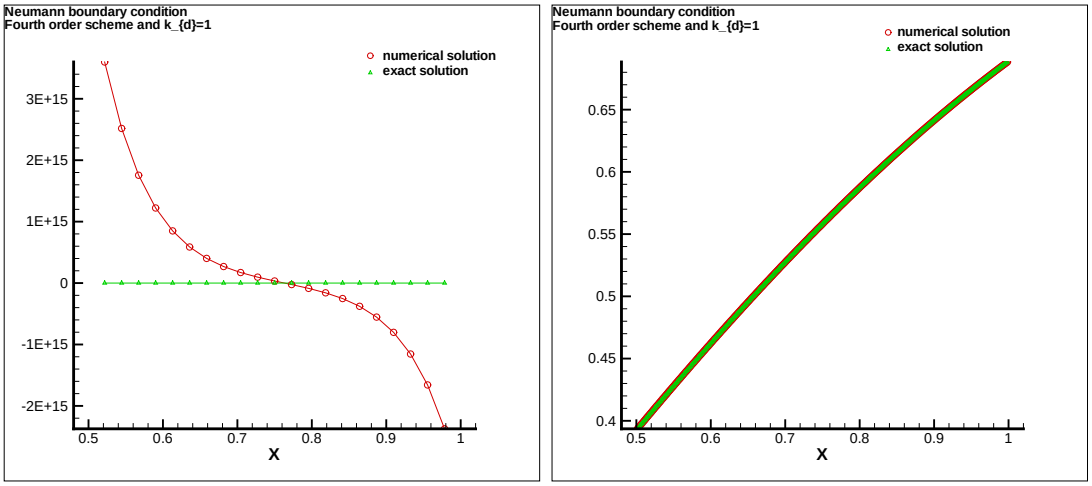

Fig. 4.12. Numerical results for (4.1) and (4.3) obtained with the fourth order scheme and the SILW procedure with $k_d = 1$. $C_a = C_b = 0.949$ with $t_{end} = 0.2$. Left: $\alpha = 0.95$ with $N = 20$ grid points; Right: $\alpha = 0.94$ with $N = 320$ grid points.

We also performed numerical tests for the case with $k_d = 2$ and have obtained the corresponding results as predicted by the analysis. We will not present the results here to save space.

Similarly, for the remaining sixth order scheme, eighth order scheme and tenth order scheme, we only give the results for the minimum value of k_d which ensures stability.

• The sixth order scheme

In this case, the minimum value of k_d is 1. Stability-instability results are given in Figs. 4.13 and 4.14. These results are consistent with the analysis.

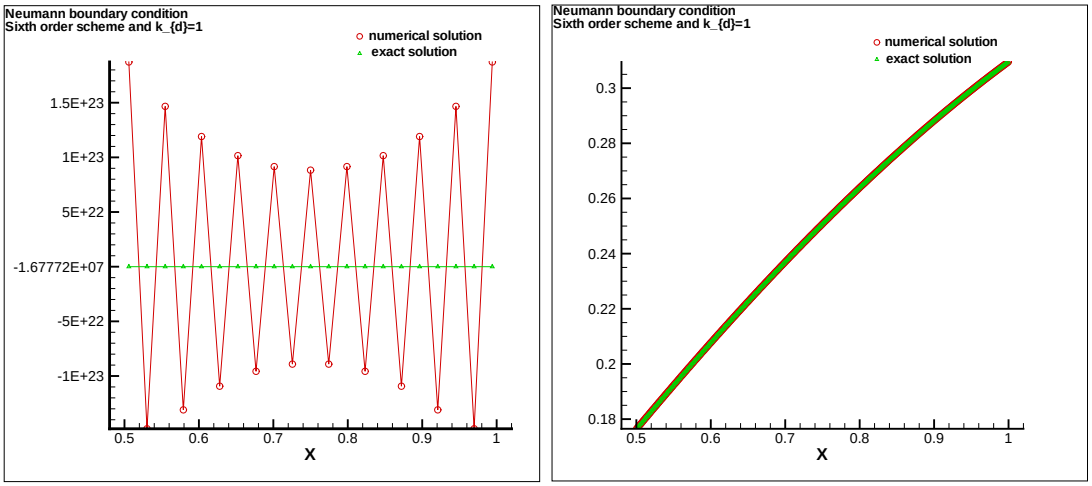

Fig. 4.13. Numerical results for (4.1) and (4.3) obtained with the sixth order scheme and the SILW procedure with $k_d = 1$. $C_a = C_b = 0.24$ with $t_{end} = 1.0$. Left: $\alpha = 0.24$ with $N = 20$ grid points; Right: $\alpha = 0.25$ with $N = 320$ grid points.

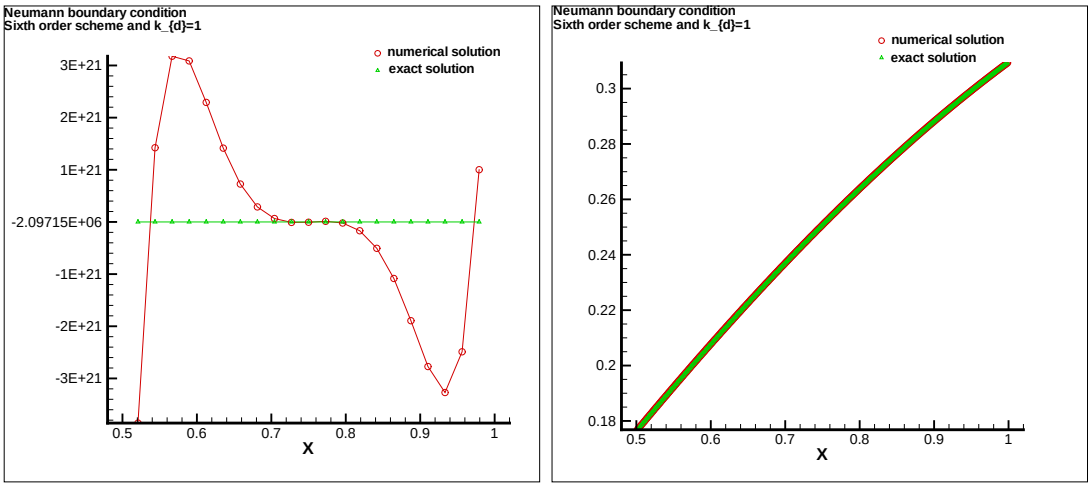

Fig. 4.14. Numerical results for (4.1) and (4.3) obtained with the sixth order scheme and the SILW procedure with $k_d = 1$. $C_a = C_b = 0.909$ with $t_{end} = 1.0$. Left: $\alpha = 0.91$ with $N = 20$ grid points; Right: $\alpha = 0.90$ with $N = 320$ grid points.

- The eighth order scheme

We repeat our numerical experiment with the eighth order scheme. In this case, the minimum value of k_d is 1. Stability-instability results are given in Figs. 4.15 and 4.16. The results are again consistent with the analysis.

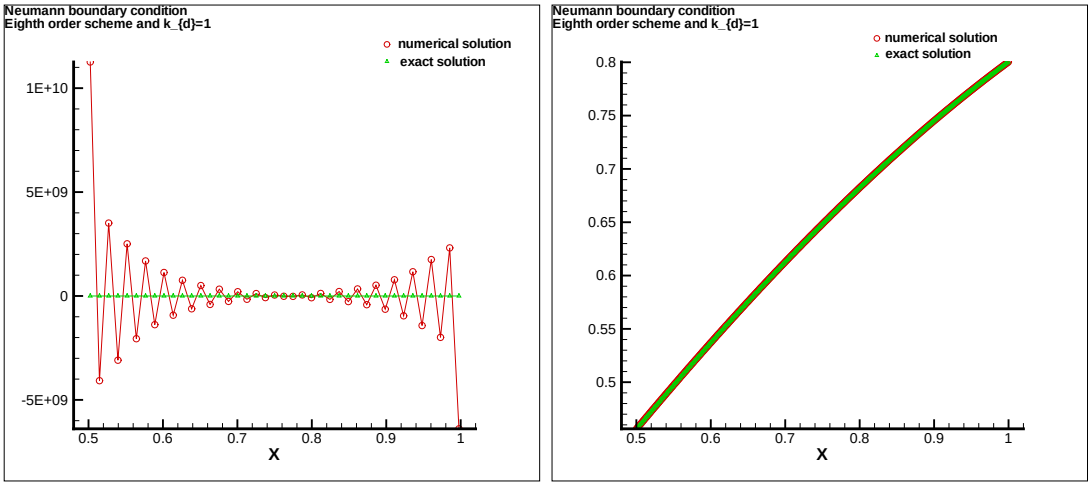

Fig. 4.15. Numerical results for (4.1) and (4.3) obtained with the eighth order scheme and the SILW procedure with $k_d = 1$. $C_a = C_b = 0.19$ with $t_{end} = 0.05$. Left: $\alpha = 0.19$ with $N = 40$ grid points; Right: $\alpha = 0.20$ with $N = 320$ grid points.

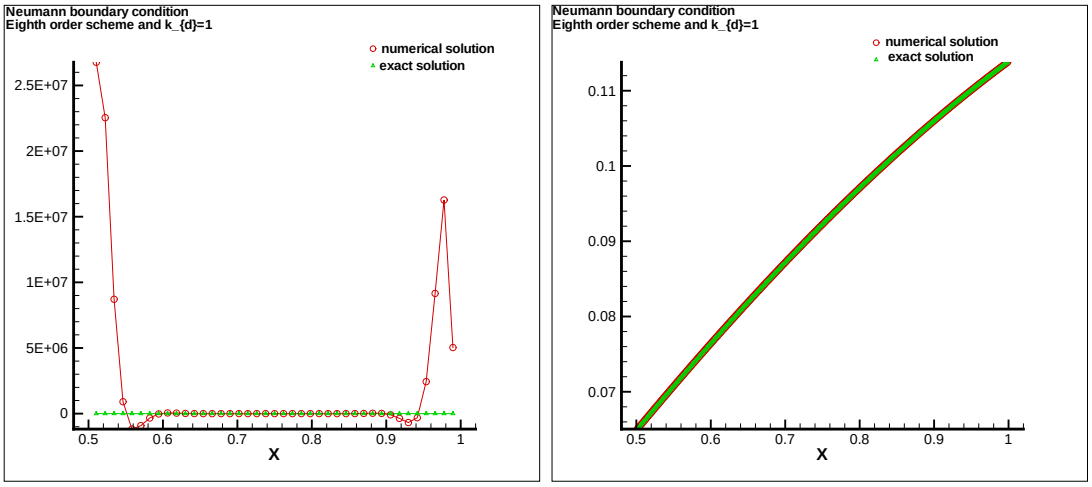

Fig. 4.16. Numerical results for (4.1) and (4.3) obtained with the eighth order scheme and the SILW procedure with $k_d = 1$. $C_a = C_b = 0.869$ with $t_{end} = 2.0$. Left: $\alpha = 0.87$ with $N = 40$ grid points; Right: $\alpha = 0.86$ with $N = 320$ grid points.

- The tenth order scheme

In this case, the minimum value of k_d is 1. Stability-instability results are given in Figs. 4.17 and 4.18.

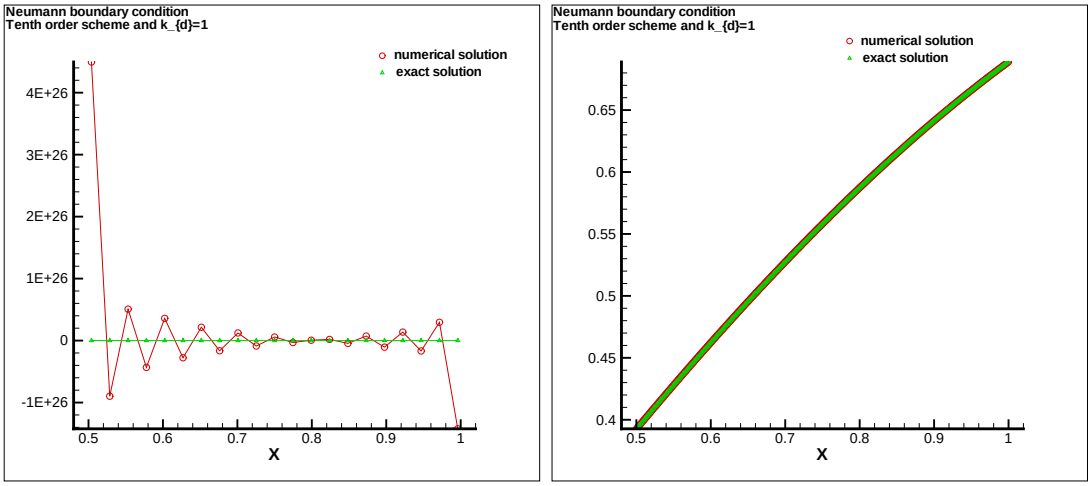

Fig. 4.17. Numerical results for (4.1) and (4.3) obtained with the tenth order scheme and the SILW procedure with $k_d = 1$. $C_a = C_b = 0.16$ with $t_{end} = 0.2$. Left: $\alpha = 0.16$ with $N = 20$ grid points; Right: $\alpha = 0.17$ with $N = 320$ grid points.

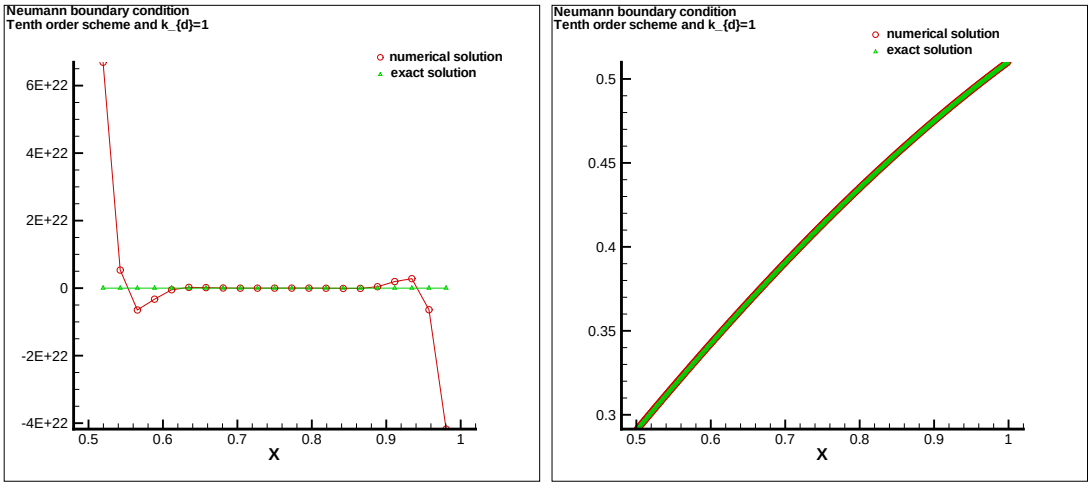

Fig. 4.18. Numerical results for (4.1) and (4.3) obtained with the tenth order scheme and the SILW procedure with $k_d = 1$. $C_a = C_b = 0.849$ with $t_{end} = 0.5$. Left: $\alpha = 0.85$ with $N = 20$ grid points; Right: $\alpha = 0.84$ with $N = 320$ grid points.

4.2 Example 2

In this subsection, we consider another example with variable coefficient.

The example is

$$\begin{cases} u_t = 2(t+1)\ u_{xx},\ \ x \in [\frac{1}{2}, 1],\ \ t \geq 0 \\ \textit{boundary conditions} \\ u(x,0) = e^{-1}\sin(x),\ \ x \in [\frac{1}{2}, 1] \end{cases} \tag{4.5}$$

The corresponding Dirichlet boundary conditions are

$$\begin{cases} u(\frac{1}{2},t) = e^{-(t+1)^2}\sin(\frac{1}{2}) \\ u(1,t) = e^{-(t+1)^2}\sin(1.0) \end{cases} \tag{4.6}$$

The corresponding Neumann boundary conditions are

$$\begin{cases} u_x(\frac{1}{2},t) = e^{-(t+1)^2}\cos(\frac{1}{2}) \\ u_x(1,t) = e^{-(t+1)^2}\cos(1.0) \end{cases} \tag{4.7}$$

The exact solution is

$$u(x,t) = e^{-(t+1)^2}\sin(x)$$

The time step size Δt is chosen as

$$\Delta t = \frac{(\lambda_{cfl})_{\max}\Delta x^2}{2(t+1)} \tag{4.8}$$

In order to save space, we only give the results of the fourth order scheme and the SILW procedure with $k_d = 1$.

4.2.1 Results for the Dirichlet boundary conditions

The computational results are given in Tables 4.7–4.9. These tables indicate stable results and the fourth order accuracy, which are consistent with the analysis.

Table 4.7. The fourth order scheme with $k_d = 1$, $\alpha = 0.67$, $t_{end} = 1.0$ for (4.5) and (4.6) with (4.8).

N	$C_a = 10^{-6}$, $C_b = 0.99999$				$C_a = 0.669$, $C_b = 0.671$			
	L^2 *error*	order	L^∞ *error*	order	L^2 *error*	order	L^∞ *error*	order
10	1.243E-08	–	3.115E-08	–	3.818E-09	–	9.817E-09	–
20	8.625E-10	3.849	2.255E-09	3.788	2.859E-10	3.739	7.576E-10	3.696
40	5.671E-11	3.927	1.519E-10	3.892	1.956E-11	3.870	5.270E-11	3.845
80	3.634E-12	3.964	9.855E-12	3.946	1.278E-12	3.935	3.476E-12	3.922

4.2.2 Results for the Neumann boundary conditions

The computational results are given in Tables 4.10–4.12. From these tables, we can find that the scheme is stable with an appropriate value of α and we can also get the desired fourth order accuracy. These results are again consistent with the analysis.

Table 4.8. The fourth order scheme with $k_d = 1$, $\alpha = 0.82$, $t_{end} = 1.0$ for (4.5) and (4.6) with (4.8).

N	$C_a = 10^{-6}$, $C_b = 10^{-6}$				$C_a = 0.819$, $C_b = 0.821$			
	L^2 *error*	order	L^∞ *error*	order	L^2 *error*	order	L^∞ *error*	order
10	4.348E-08	–	7.090E-08	–	7.012E-10	–	1.608E-09	–
20	2.640E-09	4.042	4.516E-09	3.972	6.031E-11	3.539	1.502E-10	3.421
40	1.625E-10	4.022	2.848E-10	3.987	4.485E-12	3.749	1.173E-11	3.678
80	1.007E-11	4.011	1.788E-11	3.994	3.070E-13	3.869	8.210E-13	3.837

Table 4.9. The fourth order scheme with $k_d = 1$, $\alpha = 0.96$, $t_{end} = 1.0$ for (4.5) and (4.6) with (4.8).

N	$C_a = 0.99999$, $C_b = 0.99999$				$C_a = 0.959$, $C_b = 0.961$			
	L^2 *error*	order	L^∞ *error*	order	L^2 *error*	order	L^∞ *error*	order
10	2.455E-09	–	4.149E-09	–	3.763E-09	–	6.602E-09	–
20	2.226E-10	3.463	3.795E-10	3.451	3.282E-10	3.519	5.676E-10	3.540
40	1.698E-11	3.713	2.913E-11	3.703	2.446E-11	3.746	4.180E-11	3.763
80	1.177E-12	3.851	2.029E-12	3.844	1.673E-12	3.869	2.848E-12	3.876

Table 4.10. The fourth order scheme with $k_d = 1$, $\alpha = 0.27$, $t_{end} = 1.0$ for (4.5) and (4.7) with (4.8).

N	$C_a = 10^{-6}$, $C_b = 10^{-6}$				$C_a = 0.269$, $C_b = 0.271$			
	L^2 *error*	order	L^∞ *error*	order	L^2 *error*	order	L^∞ *error*	order
10	4.033E-07	–	5.554E-07	–	1.105E-06	–	1.535E-06	–
20	3.003E-08	3.747	4.217E-08	3.719	7.797E-08	3.824	1.095E-07	3.809
40	2.020E-09	3.894	2.867E-09	3.879	5.180E-09	3.912	7.316E-09	3.904
80	1.306E-10	3.951	1.864E-10	3.943	3.338E-10	3.956	4.728E-10	3.952
160	8.338E-12	3.970	1.193E-11	3.966	2.117E-11	3.979	3.002E-11	3.977

Table 4.11. The fourth order scheme with $k_d = 1$, $\alpha = 0.60$, $t_{end} = 1.0$ for (4.5) and (4.7) with (4.8).

N	$C_a = 10^{-6}$, $C_b = 0.99999$				$C_a = 0.599$, $C_b = 0.601$			
	L^2 *error*	order	L^∞ *error*	order	L^2 *error*	order	L^∞ *error*	order
10	1.421E-06	–	2.013E-06	–	1.617E-06	–	2.315E-06	–
20	1.067E-07	3.735	1.513E-07	3.734	1.300E-07	3.637	1.854E-07	3.643
40	7.334E-09	3.863	1.040E-08	3.863	9.259E-09	3.811	1.318E-08	3.815
80	4.809E-10	3.931	6.817E-10	3.931	6.187E-10	3.904	8.794E-10	3.905
160	3.069E-11	3.970	4.350E-11	3.970	4.014E-11	3.946	5.703E-11	3.947

Table 4.12. The fourth order scheme with $k_d = 1$, $\alpha = 0.94$, $t_{end} = 1.0$ for (4.5) and (4.7) with (4.8).

N	$C_a = 0.99999$, $C_b = 0.99999$				$C_a = 0.939$, $C_b = 0.941$			
	L^2 *error*	order	L^∞ *error*	order	L^2 *error*	order	L^∞ *error*	order
10	1.329E-07	–	1.997E-07	–	1.718E-04	–	2.534E-04	–
20	1.402E-08	3.245	2.062E-08	3.276	1.570E-05	3.452	2.275E-05	3.478
40	1.154E-09	3.602	1.678E-09	3.619	1.201E-06	3.708	1.724E-06	3.722
80	8.322E-11	3.794	1.203E-10	3.803	8.333E-08	3.849	1.190E-07	3.857
160	5.735E-12	3.859	8.260E-12	3.864	5.491E-09	3.924	7.820E-09	3.927

5 Concluding remarks

In this paper, stability analysis is performed on the high order central difference schemes for solving diffusion equations with both Dirichlet and Neumann boundary conditions on a finite domain. The simplified inverse Lax-Wendroff (SILW) procedure is used to evaluate the values of the solution at the ghost points. This type of SILW boundary treatment has been proved to maintain stability and the order of accuracy, with the same CFL number $(\lambda_{cfl})_{\max}$ as in the periodic case with appropriate choice of the threshold k_d (number of terms using the inverse Lax-Wendroff procedure) and α (which separates two different ways of performing extrapolation), for any of the high order schemes presented and for all $C_a \in [0, 1)$ and $C_b \in [0, 1)$, which measure the distances of the first grid point to the physical boundary. Ranges of α for different k_d to guarantee stability for different orders of accuracy and different boundary conditions are given in Tables 3.2 and 3.3 under the $(\lambda_{cfl})_{\max}$ given by Table 3.1. Numerical examples are provided to demonstrate stability or instability predicted by the analysis in Tables 3.2 and 3.3. Two different methods, the GKS analysis and eigenvalue spectrum visualization method, are used to analyze stability in this paper. The GKS analysis breaks the problems into the summation of three simpler problems. But it could be algebraically highly complicated, particularly for high order schemes. The eigenvalue spectrum visualization method transforms the scheme to a matrix form, containing both

boundary conditions. It is algebraically simpler and easier to perform on high order schemes. Numerical tests indicate that these two methods yield consistent results. The results of this paper are expected to provide valuable guidance to users of high order central difference schemes, for solving diffusion equations over a domain for which the physical boundary does not coincide with grid points. In the future, we will extend this analysis to the methods in [14] for convection-diffusion equations. We remark that an alternative approach for the stability analysis of problems considered in this paper is via the energy method as in [20], through establishing semi-boundedness of the spatial operator, which contains the influence of boundaries. This might involve the design of suitable weights in the definition of the norm taking into account the specific boundary treatments. It would be an interesting topic to pursue in the future.

Acknowledgment: We thank one of the referees for giving the remark about the alternative approach for the stability analysis at the end of the concluding remarks section.

References

[1] M.J. Berger, C. Helzel and R.J. LeVeque, *h-box methods for the approximation of hyperbolic conservation laws on irregular grids*, SIAM Journal on Numerical Analysis, 41:893–918, 2003.

[2] M.H. Carpenter, D. Gottlieb, S. Abarbanel and W.-S. Don, *The theoretical accuracy of Runge-Kutta time discretizations for the initial boundary value problem: a study of the boundary error*, SIAM Journal on Scientific Computing, 16:1241-1252, 1995.

[3] M. Goldberg and E. Tadmor, *Scheme-independent stability criteria for difference approximations of hyperbolic initial-boundary value problems. I*, Mathematics of Computation, 32:1097–1107, 1978.

[4] M. Goldberg and E. Tadmor, *Scheme-independent stability criteria for difference approximations of hyperbolic initial-boundary value problems. II*, Mathematics of Computation, 36:603–626, 1981.

[5] B. Gustafsson, H.-O. Kreiss and A. Sundström, *Stability theory of difference approximations for mixed initial boundary value problem. II*, Mathematics of Computation, 26:649–686, 1972.

[6] W.D. Henshaw, *A high-order accurate parallel solver for Maxwell's equations on overlapping grids*, SIAM Journal on Scientific Computing, 28:1730–1765, 2006.

[7] W.D. Henshaw, H.-O. Kreiss and L.G.M. Reyna, *A fourth-order accurate difference approximation for the incompressible Navier-Stokes equations*, Computers & Fluids, 23:575–593, 1994.

[8] L. Huang, C.-W. Shu and M. Zhang, *Numerical boundary conditions for the fast sweeping high order WENO methods for solving the Eikonal equation*, Journal of Computational Mathematics, 26:336–346, 2008.

[9] H.-O. Kreiss and N.A. Petersson, *A second order accurate embedded boundary method for the wave equation with Dirichlet data*, SIAM Journal on Scientific Computing, 27:1141–1167, 2006.

[10] H.-O. Kreiss, N.A. Petersson and J. Yström, *Difference approximations for the second order wave equation*, SIAM Journal on Numerical Analysis, 40: 1940–1967, 2002.

[11] H.-O. Kreiss, N.A. Petersson and J. Yström, *Difference approximations of the Neumann problem for the second order wave equation*, SIAM Journal on Numerical Analysis, 42:1292–1323, 2004.

[12] T. Li, C.-W. Shu and M. Zhang, *Stability analysis of the inverse Lax-Wendroff boundary treatment for high order upwind-biased finite difference schemes*, Journal of Computational and Applied Mathematics, 299:140–158, 2016.

[13] Y. Liu, C.-W. Shu and M. Zhang, *High order finite difference WENO schemes for nonlinear degenerate parabolic equations*, SIAM Journal on Scientific Computing, 33:939–965, 2011.

[14] J. Lu, J. Fang, S. Tan, C.-W. Shu and M. Zhang, *Inverse Lax-Wendroff procedure for numerical boundary conditions of convection-diffusion equations*, Journal of Computational Physics, 317:276–300, 2016.

[15] S. Osher, *Stability of parabolic difference approximations to certain mixed initial boundary value problems*, Mathematics of Computation, 26:13–39, 1972.

[16] C.-W. Shu and S. Osher, *Efficient implementation of essentially non-oscillatory shock-capturing schemes*, Journal of Computational Physics, 77:439–471, 1988.

[17] B. Sjögreen and N.A. Petersson, *A Cartesian embedded boundary method for hyperbolic conservation laws*. Communications in Computational Physics, 2:1199–1219, 2007.

[18] E. Sousa, *Stability analysis of difference methods for parabolic initial value problems*, Journal of Scientific Computing, 26:45–66, 2006.

[19] J.C. Strikwerda, *Initial boundary value problems for the method of lines*, Journal of Computational Physics, 34:94–107, 1980.

[20] E. Tadmor, *From semi-discrete to fully discrete: stability of Runge-Kutta schemes by the energy method. II*, in "Collected Lectures on the Preservation of Stability under Discretization", D. Estep and S. Tavener, eds. Proceedings in Applied Mathematics 109, SIAM 2002, 25–49.

[21] S. Tan and C.-W. Shu, *Inverse Lax-Wendroff procedure for numerical boundary conditions of conservation laws*, Journal of Computational Physics, 229:8144–8166, 2010.

[22] S. Tan and C.-W. Shu, *A high order moving boundary treatment for compressible inviscid flows*, Journal of Computational Physics, 230:6023–6036, 2011.

[23] S. Tan, C. Wang, C.-W. Shu and J. Ning, *Efficient implementation of high order inverse Lax-Wendroff boundary treatment for conservation laws*, Journal of Computational Physics, 231:2510–2527, 2012.

[24] J.M. Varah, *Stability of difference approximations to the mixed initial boundary value problems for parabolic systems*, SIAM Journal on Numerical Analysis, 8:598–615, 1971.

[25] F. Vilar and C.-W. Shu, *Development and stability analysis of the inverse Lax-Wendroff boundary treatment for central compact schemes*, Mathematical Modelling and Numerical Analysis, 49:39–67, 2015.